(2)

AFWAL-TR-84-3028

TWO-PHASE FLUID THERMAL TRANSPORT FOR SPACECRAFT

Robert E. Eastman
Carl J. Feldmanis
William L. Haskin
Kent L. Weaver

Vehicle Equipment Division
Flight Dynamics Laboratory

October 1984

Final Report for Period 1 October 1982 - 30 September 1983

Approved for public release; distribution unlimited.

FLIGHT DYNAMICS LABORATORY
AIR FORCE WRIGHT AERONAUTICAL LABORATORIES
AIR FORCE SYSTEMS COMMAND
WRIGHT-PATTERSON AIR FORCE BASE, OHIO 45433

NOTICE

When Government drawings, specifications, or other data are used for any purpose other than in connection with a definitely related Government procurement operation, the United States Government thereby incurs no responsibility nor any obligation whatsoever; and the fact that the government may have formulated, furnished, or in any way supplied the said drawings, specifications, or other data, is not to be regarded by implication or otherwise as in any manner licensing the holder or any other person or corporation, or conveying any rights or permission to manufacture use, or sell any patented invention that may in any way be related thereto.

This report has been reviewed by the Office of Public Affairs (ASD/PA) and is releasable to the National Technical Information Service (NTIS). At NTIS, it will be available to the general public, including foreign nations.

This technical report has been reviewed and is approved for publication.

Robert E. Eastman

ROBERT E. EASTMAN, 1Lt, USAF
Project Engineer

William L. Haskin

WILLIAM L. HASKIN
Project Engineer

FOR THE COMMANDER

Arnold H. Mayer

ARNOLD H. MAYER
Asst. for Research & Technology
Vehicle Equipment Division
Flight Dynamics Laboratory

"If your address has changed, if you wish to be removed from our mailing list, or if the addressee is no longer employed by your organization please notify AFWAL/FIEE, *W-PAFB, OH 45433 to help us maintain a current mailing list".*

Copies of this report should not be returned unless return is required by security considerations, contractual obligations, or notice on a specific document.

UNCLASSIFIED

SECURITY CLASSIFICATION OF THIS PAGE *(When Data Entered)*

REPORT DOCUMENTATION PAGE	READ INSTRUCTIONS BEFORE COMPLETING FORM
1. REPORT NUMBER AFWAL-TR-84-3028	2. GOVT ACCESSION NO. A151316 3. RECIPIENT'S CATALOG NUMBER
4. TITLE *(and Subtitle)* TWO-PHASE FLUID THERMAL TRANSPORT FOR SPACECRAFT	5. TYPE OF REPORT & PERIOD COVERED Final Report Oct 82 - Sept 83
	6. PERFORMING ORG. REPORT NUMBER
7. AUTHOR(s) Robert E. Eastman, Carl J. Feldmanis, William L. Haskin, Kent L. Weaver	8. CONTRACT OR GRANT NUMBER(s)
9. PERFORMING ORGANIZATION NAME AND ADDRESS Flight Dynamics Laboratory (AFWAL/FIEE) Air Force Wright Aeronautical Laboratories (AFSC) Wright-Patterson Air Force Base, OH 45433	10. PROGRAM ELEMENT, PROJECT, TASK AREA & WORK UNIT NUMBERS Program Element 61102F Project 2308, Task N1 Work Unit 2308N102
11. CONTROLLING OFFICE NAME AND ADDRESS Flight Dynamics Laboratory (AFWAL/FIEE) Air Force Wright Aeronautical Laboratories (AFSC) Wright-Patterson Air Force Base, OH 45433	12. REPORT DATE October 1984 13. NUMBER OF PAGES 101
14. MONITORING AGENCY NAME & ADDRESS*(if different from Controlling Office)*	15. SECURITY CLASS. *(of this report)* UNCLASSIFIED 15a. DECLASSIFICATION DOWNGRADING SCHEDULE

16. DISTRIBUTION STATEMENT *(of this Report)*

Approved for public release; distribution unlimited.

17. DISTRIBUTION STATEMENT *(of the abstract entered in Block 20, if different from Report)*

18. SUPPLEMENTARY NOTES

19. KEY WORDS *(Continue on reverse side if necessary and identify by block number)*

Two-phase fluid flow
Two-phase heat transfer
Boiling
Condensing
Flow patterns
Spacecraft thermal control
Spacecraft subsystems

20. ABSTRACT *(Continue on reverse side if necessary and identify by block number)*

Many future space satellites for surveillance and defense missions will have five to twenty times higher internal heat generation rates than satellites presently being launched. Efficient and effective methods of collecting, transporting, and rejecting this thermal energy must be developed to assure mission success within overall system constraints. One concept for more effective thermal transport would replace ordinary, single-phase liquid circulating loops with two-phase (liquid-vapor) loops. This would allow use

DD FORM 1 JAN 73 1473 EDITION OF 1 NOV 65 IS OBSOLETE

UNCLASSIFIED

SECURITY CLASSIFICATION OF THIS PAGE *(When Data Entered)*

20. (continued)

of the latent heat of vaporization so that flow rates would be sharply reduced, temperature drops would be very small, and heat transfer coefficients could be large compared to single-phase fluid forced convection. The thermal transport cabability of pumped two-phase loops can also be made much larger than that of conventional heat pipes.

Hindering the development of two-phase fluid heat transfer systems is the fact that ground test data cannot presently be used to accurately predict two-phase fluid pressure changes and heat transfer coefficients for space flight conditions where the influence of the gravity force is absent. This is due to a lack of detailed knowledge of the effects of various forces on the fluid flow regimes and heat transfer mechanisms. The research effort described in this report was conducted to begin an analysis of the phase change and flow processes of interest for spacecraft thermal transport loops. Pertinent literature was examined to identify the limits of existing theory and experimental results. It was found that data from low gravity force experiments are very limited, and much of this data is not adequately explained by existing analytical methods.

The basic process of bubble growth in a liquid was analyzed, and good correlation was obtained with previous experimental data of other investigators. An expanded explanation of the forces causing bubble separation from a heated surface indicates conditions under which pool boiling may be possible in a weightless environment.

Standard equations for pressure gradients and heat transfer coefficients in boiling and condensing systems were assembled as a starting point for further analysis. Criteria for predicting flow pattern boundaries were also reviewed, and implications for low effective gravity environments are discussed.

Finally, initial concepts for two-phase heat transfer loops on a spacecraft are briefly discussed with indications of the need for continued analytical and experimental work.

PREFACE

The analysis described in this report was done in response to a need to begin to develop more efficient and more effective heat transfer methods for use on future military space vehicles. The work was conducted by personnel in the Environmental Control Branch of the Vehicle Equipment Division of the Flight Dynamics Laboratory at Wright-Patterson Air Force Base. The effort was partially sponsored by the Air Force Office of Scientific Research (AFOSR/NA) as Task No. 2308N2. Additional work based on the studies reported here is being done in the Flight Dynamics Laboratory under Project 2402, Work Unit No. 24020450.

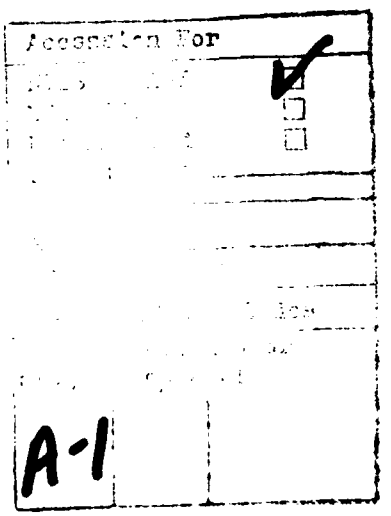

TABLE OF CONTENTS

LIST OF ILLUSTRATIONS

LIST OF ILLUSTRATIONS (Concluded)

LIST OF SYMBOLS
(BOTH ENGLISH AND METRIC UNITS ARE USED)

$c_{p\,\ell}$	specific heat of the liquid
D	diameter
D_b	diameter of the bubble base
g	local or effective gravitational acceleration
g_c	gravitational constant
G	mass velocity
J	volumetric flux
ℓ	length or a subscript for liquid
L	heat of vaporization or a subscript for liquid
M	mass
Nu	Nusselt number
P	pressure
Pr	prandtl number
Q	heat input
Q"	heat flux
R	radius
R_b	bubble base radius
R_o	critical radius
R_{fc}	radius of most favorable cavity
Re	Reynolds number
t	time
T_w	wall temperature
T_{sat}	saturation temperature (T_s also used)
T	bulk fluid temperature
u	velocity

LIST OF SYMBOLS (Concluded)

ν	specific volume of the vapor
v	volume
$\dot{w}$	mass flow rate
V_{bub}	volume of bubble
α	thermal diffusivity or void fraction
δ	thermal boundry layer thickness
μ_ℓ	liquid viscosity
μ_w	liquid viscosity at wall
ν_ℓ	liquid kinematic viscosity
ρ_ℓ	liquid density
ρ_v	vapor density
σ	surface tension
Θ	contact angle between bubble and wall

SECTION I

INTRODUCTION

1. BACKGROUND

a. Spacecraft Thermal Transport Requirements

If mass expulsion systems are excluded, all energy dissipated on a space satellite must be transported to an external surface and rejected by radiation. Most present-day satellites operate with power levels below one kilowatt while a few have power levels up to four kilowatts. However, many near-future satellites for surveillance and defense missions will have power requirements of five to ten kilowatts. This requirement is expected to grow to 100 KW or more (Reference 1) during the next twenty years. Transport distances between heat sources and radiators could vary from one to fifty meters depending on spacecraft size and configuration. Thus, a transport capability of up to 5,000,000 watt-meters may be needed. Operating temperature for electronic equipment will probably be in the 0-40°C (32-104°F) range with an operating life of seven to ten years expected. Presently used spacecraft thermal control methods, as described in the next paragraph, are not adequate for these future transport requirements.

b. Present Thermal Control Methods

Traditionally, spacecraft thermal designs have been based on cold bias/passive thermal control techniques; that is, payload components are designed to tolerate large temperature swings and high temperature operation. Excess heat from these power dissipating components is transferred by solid conductors and internal radiation to outer surfaces for radiation to space. Under-temperature operation is prevented by component heaters at the expense of parasitic power penalties (to 40% of the required total spacecraft power). The growth of these parasitic power penalties to achieve thermal control is a discomforting trend, from both a heater complexity/reliability and power system weight penalty standpoint.

One device sometimes used for thermal transport on a spacecraft is the "heat pipe." Heat pipes are passive devices which can transport thermal energy with a very small temperature drop. Liquid in the heat pipe is evaporated at the warmer part of the pipe. The vapor flows to cooler regions where condensation occurs. Surface tension in a wick or porous structure causes the liquid to flow from the condenser to the evaporator by capillary action and balances the pressure drop in the vapor. Different fluids can be selected for the desired operating temperature. No pump is needed, and a nearly uniform temperature can be maintained.

The quantity of heat conducted through a heat pipe is limited by the low pressure differential which can be generated in the wick and the height to which the liquid must be lifted against gravity. Some high capacity heat pipes are being developed to transport hundreds of watts for distances up to fifty feet or thousands of watts for ten feet at ordinary temperatures, but transport of large heat loads over long distances by heat pipes cannot yet be considered an established capability.

Heat pipes can be thermally connected end to end (cascaded) so that the total length is extended, but this causes a substantial increase in the total temperature drop. Special heat pipe devices are also available for conducting heat in only one direction or controlling the temperature with varying heat inputs or sink temperatures.

Single-phase liquid or gaseous heat transfer loops have been used on some satellites when internal radiation, ordinary thermal conduction and heat pipe devices cannot provide sufficient transport capability (watt-meters). Since only the sensible heat of the circulating fluid is used, the temperature rise in the fluid and the flow rate are directly proportional to the required heat transfer rate. A large temperature rise and high pump power can result from high cooling loads. Low film coefficients in the convective heat exchangers further contribute to the inefficiencies and limit the flux available for special components.

c. Two-Phase Fluid Thermal Transport Concept

Concepts which have emerged for more effective thermal transport methods would replace the single-phase loop with two-phase (liquid-vapor) processes. This would allow use of the latent heat of vaporization so that flow rates would be sharply reduced, temperature drops would be very small, and heat transfer coefficients could be large. Much higher heat flux limits, equipment specific weights, and economies in coolant circulting requirements are possible when the restriction to single-phase transport is relaxed. Figure 1 is a schematic of a possible eventual application of the two-phase concept. In a typical comparison with a single-phase liquid loop, pump power would be reduced by two orders of magnitude, heat transfer coefficients would be 10-100 times higher, and the more uniform temperature should improve the reliability of electronic equipment. An additional benefit from the small temperature drops obtainable with the two-phase system is a heat rejection radiator temperature nearly as high as that of the source heat exchangers. Radiator area reductions made possible by relatively small temperature increases are illustrated in Figure 2.

Terrestrial applications with thermal trsnsport requirements of comparable magnitude and flux intensities, e.g., nuclear and conventional power generation and high power electron device cooling, are addressed using ebullition (boiling) cooling and two-phase (liquid-vapor) heat transport. However, use of two-phase fluids on free-flying space satellites is usually avoided because of gaps in quantitative descriptions of two-phase phenomenology important to design of the systems.

Presently, ground test data cannot be used to accurately predict two-phase fluid pressure changes and heat transfer coefficients for space flight conditions where the influence of the normal gravity force is absent. Although many two-phase fluid dynamic phenomena present in the power industries are insensitive to the effects of gravity, a wholesale transfer of terrestrial two-phase technology approaches to the weightless environment of space is not feasible. In particular, the gravity body force is important to the vapor bubble detachment process in pool

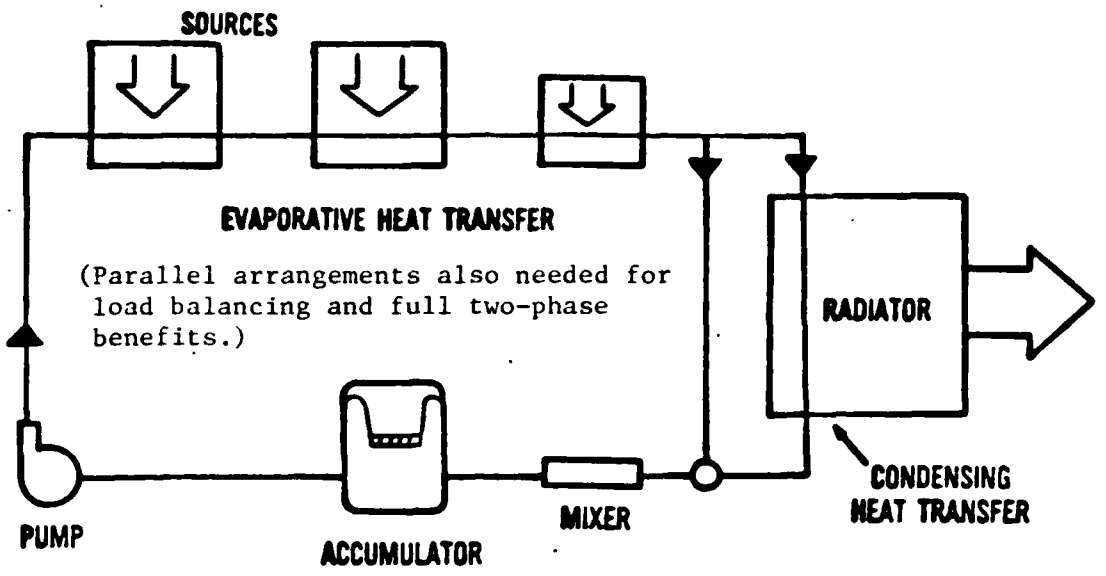

Figure 1. Two-Phase Fluid Loop Concept

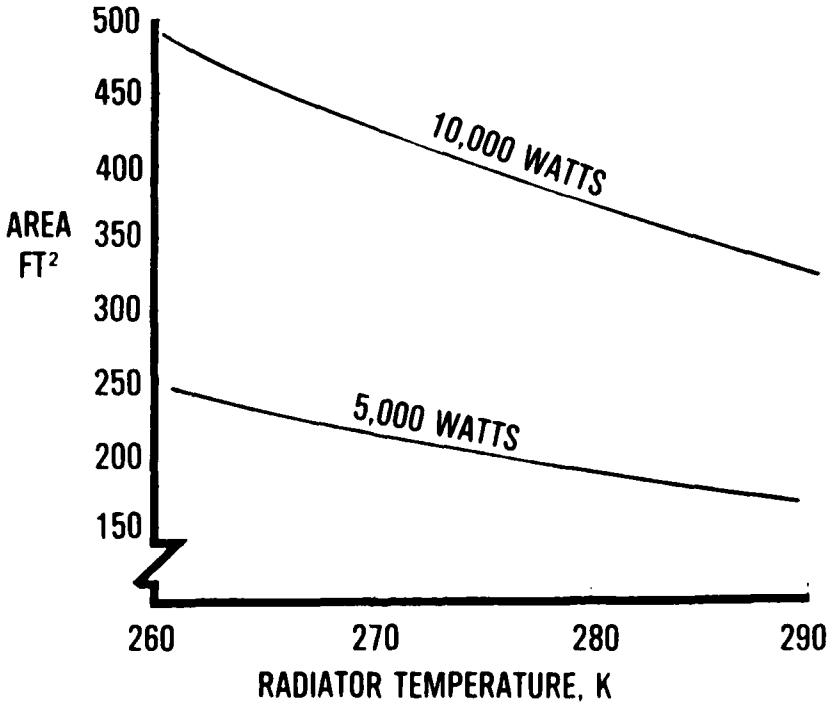

Figure 2. Typical Radiator Areas

boiling and low liquid velocity regimes. Its influence on the shape of the interface boundary and the phase dispersion topology of one phase in the other has a significant impact on achievable process technology factors such as heat transfer coefficients, pressure drops, and the potential for gross flow instabilities. Many aspects of terrestrial two-phase fluid flow and separation control approaches rely on the gravity force. These must be replaced by treatments appropriate to the weightless environment before the benefits of two-phase heat transport can become available for spacecraft applications.

NASA has begun the development of two-phase fluid thermal systems (Reference 2) for space platform applications. Annalyses and experiments are being conducted to investigate several aspects of alternate designs. Operation of a loop with five different heat exchangers in the laboratory (Reference 3) has shown the feasibility although indicating a need for cautious system design. Evaporative cold plates and other components for the loops are being developed in separate NASA-sponsored efforts.

Fundamental fluid physics and heat transfer research (Reference 4) is being conducted by NASA-Lewis Research Center. This work may eventually include space experiments for both pool boiling and convective boiling with low effective gravity forces. Data from these experiments could aid in the design of two-phase fluid heat transfer loops.

The NASA programs and the large amount of two-phase fluid research being done for applications such as terrestrial power stations provide a broad foundation of useful data. However, fundamental questions remain concerning the flow regimes and heat transfer mechanisms to be expected in the weightless environment of a space satellite. A complete understanding of the fluid behavior is needed in order to use ground test data to predict flight performance and to prevent "over-design" of the system. Therefore, an Air Force Office of Scientific Research (AFOSR) sponsored effort was conducted in the Flight Dynamics Laboratory to begin a detailed analysis of boiling, condensing, and fluid flow processes of interest for spacecraft thermal transport loops.

2. SCOPE OF EFFORT

In recognition of the need to develop more effective and efficient thermal management methods for future military spacecraft, an in-house research effort was conducted to define the scope of needed two-phase fluid work and begin an analysis of the phase change and flow processes. This work spanned the range from basic bubble growth analysis to consideration of preliminary concepts for a heat transfer loop on a satellite.

The basic process of bubble growth was analyzed, and good correlation was obtained with previous experimental data of other investigators. An improved explanation of the forces causing bubble separation from a heated surface indicates conditions under which pool boiling may be possible in a weightless environment. These conditions are described in the next section of the report.

Standard equations for pressure gradients and heat transfer coefficients in boiling and condensing systems were assembled as a starting point for further analysis. Criteria for predicting flow pattern boundaries were also reviewed, and implications for low effective gravity environments are discussed in the section following the condensation analysis.

Finally, initial concepts for two-phase heat transfer loops on a spacecraft are briefly discussed with indications of the need for continued analytical and experimental work.

SECTION II

BOILING PROCESSES

Boiling is associated with the changing of a liquid to a vapor. Extremely high heat fluxes can be achieved during this process which makes it ideal for very efficient heat transport loops. However, before effective evaporators can be built for use in space, a better understanding of the boiling phenomena is needed. This section first explains the basic mechanics of the boiling process, which involves both bubble growth and detachment from a surface. A general discussion of forced convectin boiling concludes the section.

1. GROWTH OF A VAPOR BUBBLE

The first step of understanding the boiling process is to understand how a vapor bubble grows. The following text explains this growth first for a bubble in a uniformly super-heated fluid and then for a bubble growing on a heated surface.

a. Growth of a Bubble in a Uniformly Super-heated Liquid

The equation governing the growth of a bubble is given in the literature as being the extended Rayleigh equation

$$R\ddot{R} + (3/2)\dot{R}^2 + \frac{2\sigma}{\rho_\ell R} = \frac{\Delta P}{\rho_\ell} \qquad (1)$$

where R is the bubble radius, σ is the surface tension, ρ_ℓ is the liquid density. ΔP is the absolute pressure difference between the vapor in the bubble and the liquid, and $2\sigma/R$ is the excess pressure inside the bubble caused by the surface tension of the fluid. ΔP is not constant, but varies with time.

The growth of a vapor bubble and its associated radial surface velocity and acceleration for the general case as given by Equation 1 are shown in Figure 3. It can be seen that the bubble grows slowly to a critical radius, R_o, followed by an extremely rapid growth rate which gradually tapers off.

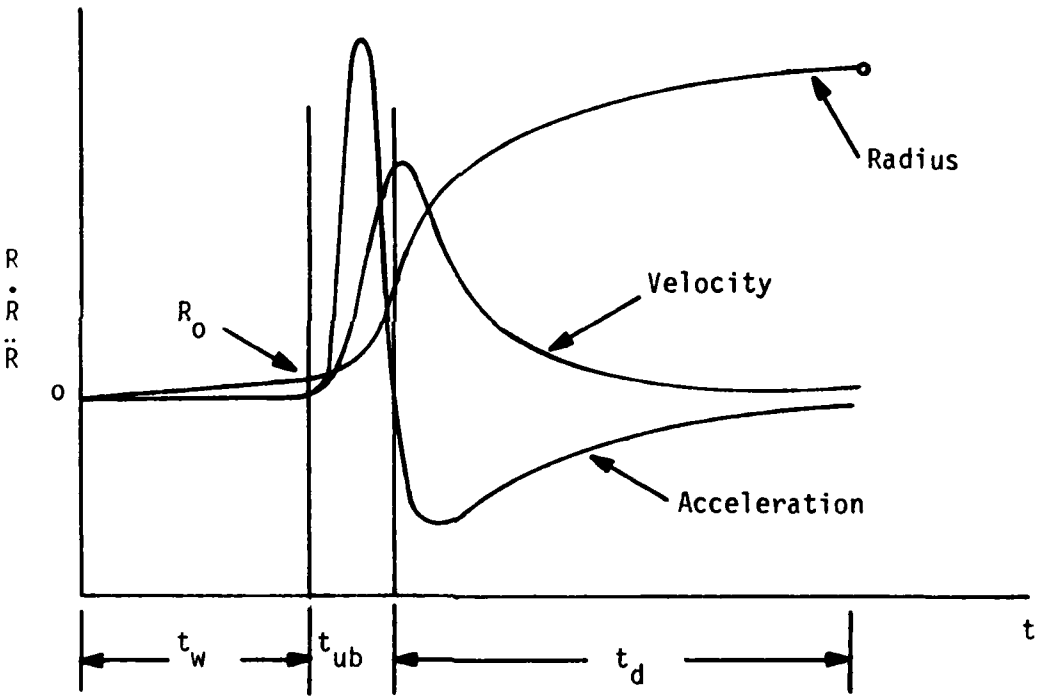

Figure 3. Bubble Growth Curves

The critical radius is (Reference 6)

$$R_o = \frac{2\sigma}{\Delta P} \tag{2}$$

which is the radius where the bubble achieves unstable equilibrium before its rapid growth stage.

The growth of a bubble can be broken down into three phases (Figure 3). The first phase, t_w, is a waiting period where the bubble slowly grows to R_o. The second phase, t_{ub}, is an explosive growth phase in which the hydrodynamic forces (right side of Equation 1) are important. This phase is extremely short. The third phase, t_d, is where the hydrodynamic forces become negligible. During this phase, the equation of growth comes down to the solution of the heat conduction equation with a moving boundary and an evaporative heat sink.

The heat conduction equation has been solved for $t > t_{ub}$ by Forster and Zuber (References 7 and 8) yielding the following equation for R:

$$\frac{R}{R_o} + \ln\left(\frac{R/R_o - 1}{.015}\right) = Ct^{1/2} \tag{3}$$

where:

$$C = \frac{\Delta T\, C_{P\ell}\, \rho_\ell\, \sqrt{\pi\alpha}}{L\rho_v\, R_o}$$

and with the constraint:

$$t > \frac{1.03}{C^2}$$

C_{P_ℓ} is the liquid specific heat, ρ_ℓ is the liquid density, ρ_v is the vapor density, L is the heat of vaporization, and α is the liquid thermal diffusivity. When R becomes an order of magnitude larger than R_o it can be approximated by:

$$R \approx \frac{\Delta T\, C_{P\ell}\, \rho_\ell\, \sqrt{\pi\alpha}}{L\rho_v}\, \sqrt{t} \tag{4}$$

The calculated growth rates for steam bubbles growing in super-heated water are shown in Figures 4, 5 and 6 for various super-heats. Experimental values are also shown. As can be seen, Equation 4 agrees very well with the experimental results.

b. Growth of a Bubble on a Heated Wall

The growth of a bubble on a heated wall is similar to growth in a superheated fluid except that it grows through a temperature gradient, and the energy for bubble growth comes from the wall rather than from the bulk of the fluid. The growth of a vapor bubble and its associated surface velocity and acceleration for the general case of growth on a heated wall are plotted in Figure 7. This figure shows that the bubble again has a slow initial growth phase t_w, where it grows to R_o. As it grows to this radius, the shape of the bubble is a hemisphere. When it reaches its explosive growth phase, or unbinding period (Reference 9) the bubble wall accelerates radially outward retaining its hemispherical shape. Finally, in the third phase where the bubble growth rate is determined by the heat conducted to the bubble wall, the bubble base width stops growing except for the thin layer that is evaporated away. The rest of the bubble expands like a balloon until it is almost spherical in shape.

Compared to a bubble in a super-heated liquid, the biggest difference for the growth of a bubble on a heated wall is that it grows through a temperature gradient. Initially, the fluid next to the wall begins to heat up forming a temperature gradient. When the fluid achieves a temperature high enough to nucleate a bubble in a given nucleation site, the bubble will begin to grow. The bubble grows slowly to R_o while the thermal boundary, δ, also continues to grow. After the bubble reaches R_o, the thermal boundary layer is carried away from the wall by the rapidly expanding bubble as shown in Figure 8. This thermal boundary layer then provides most of the energy for continued growth.

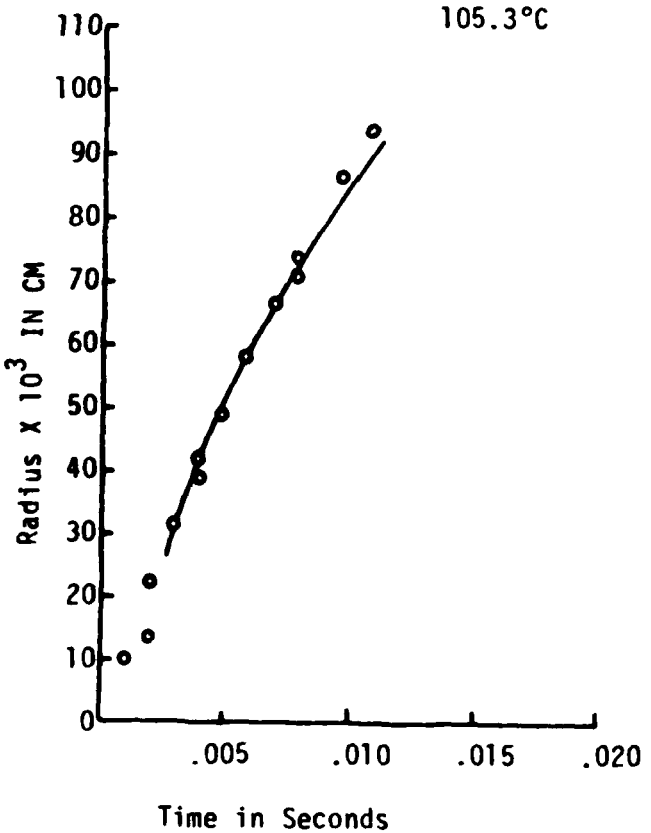

(Cracks and squares show experimental values by Plesset and Zwick)

Figure 4. 5°C Superheat

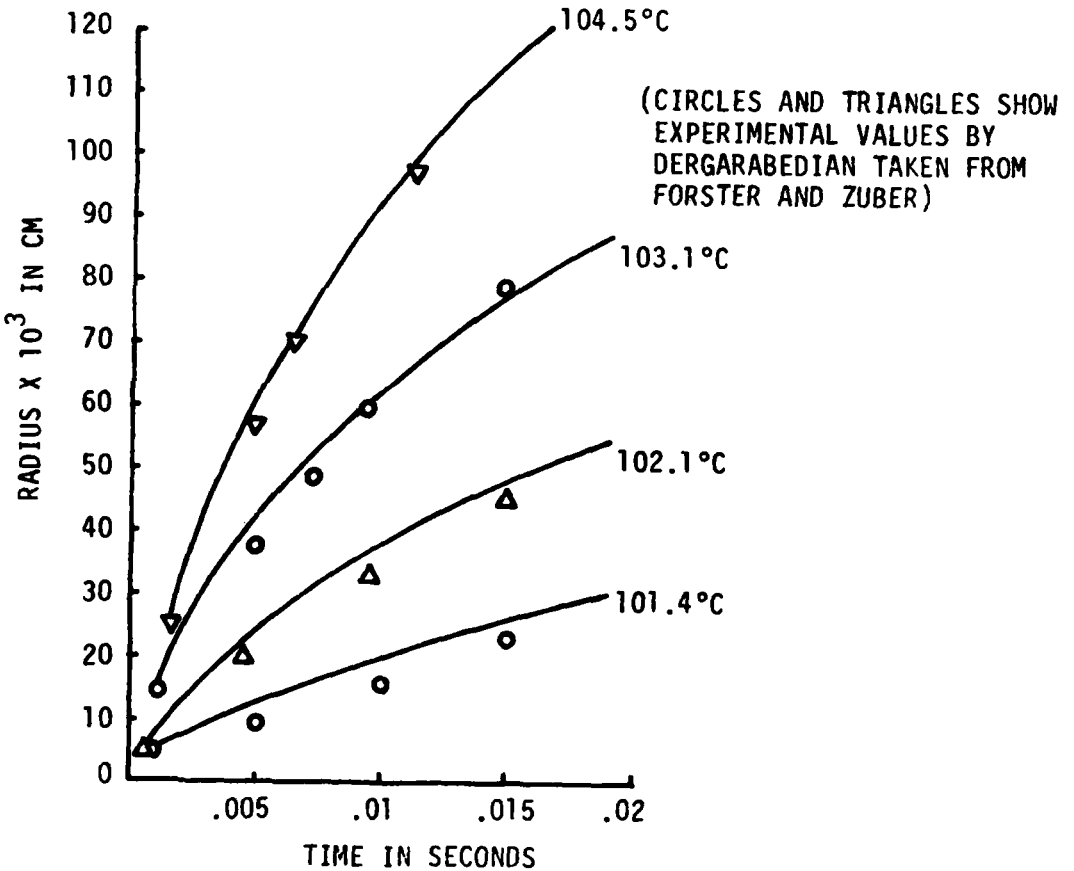

Figure 5. Various Temperatures

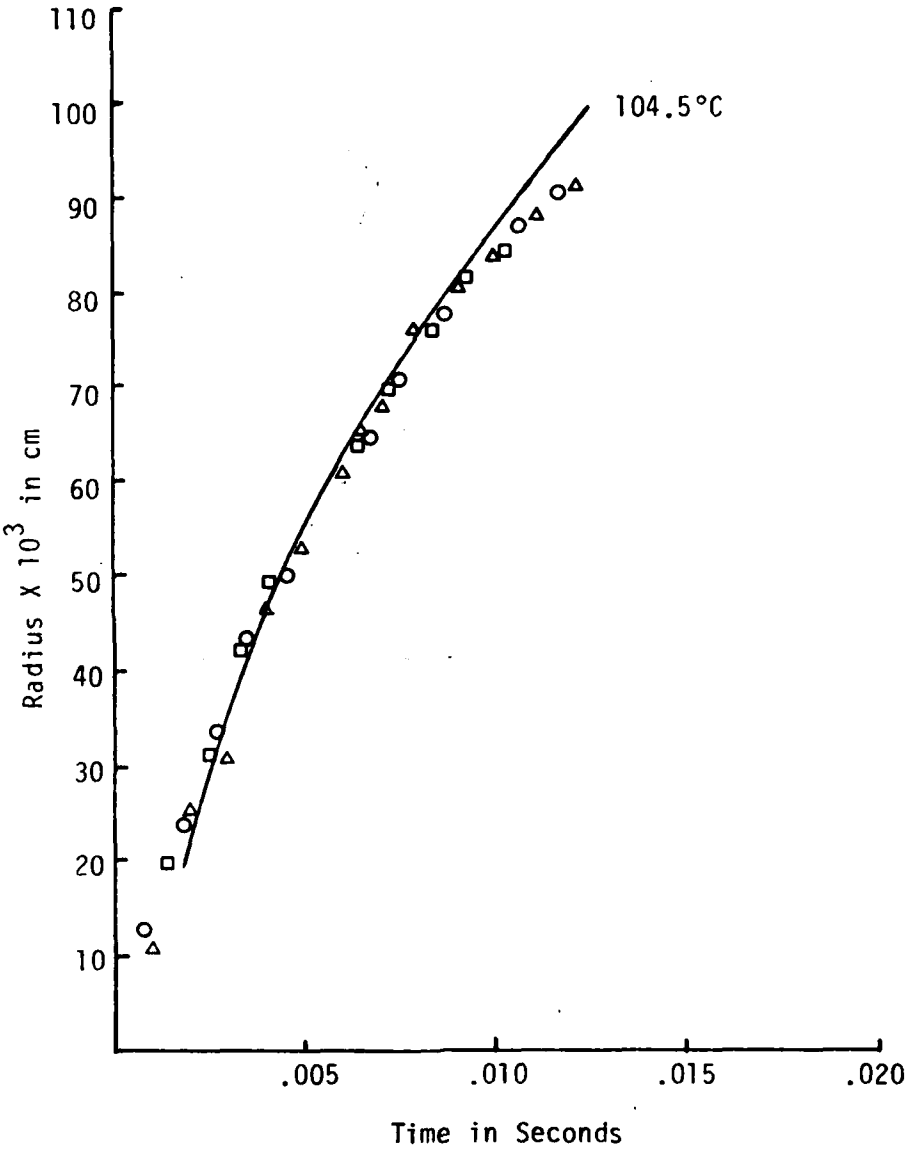

Figure 6. 4°C Superheat

(Circles, squares, and triangles show experimental values by Plesset and Zwick)

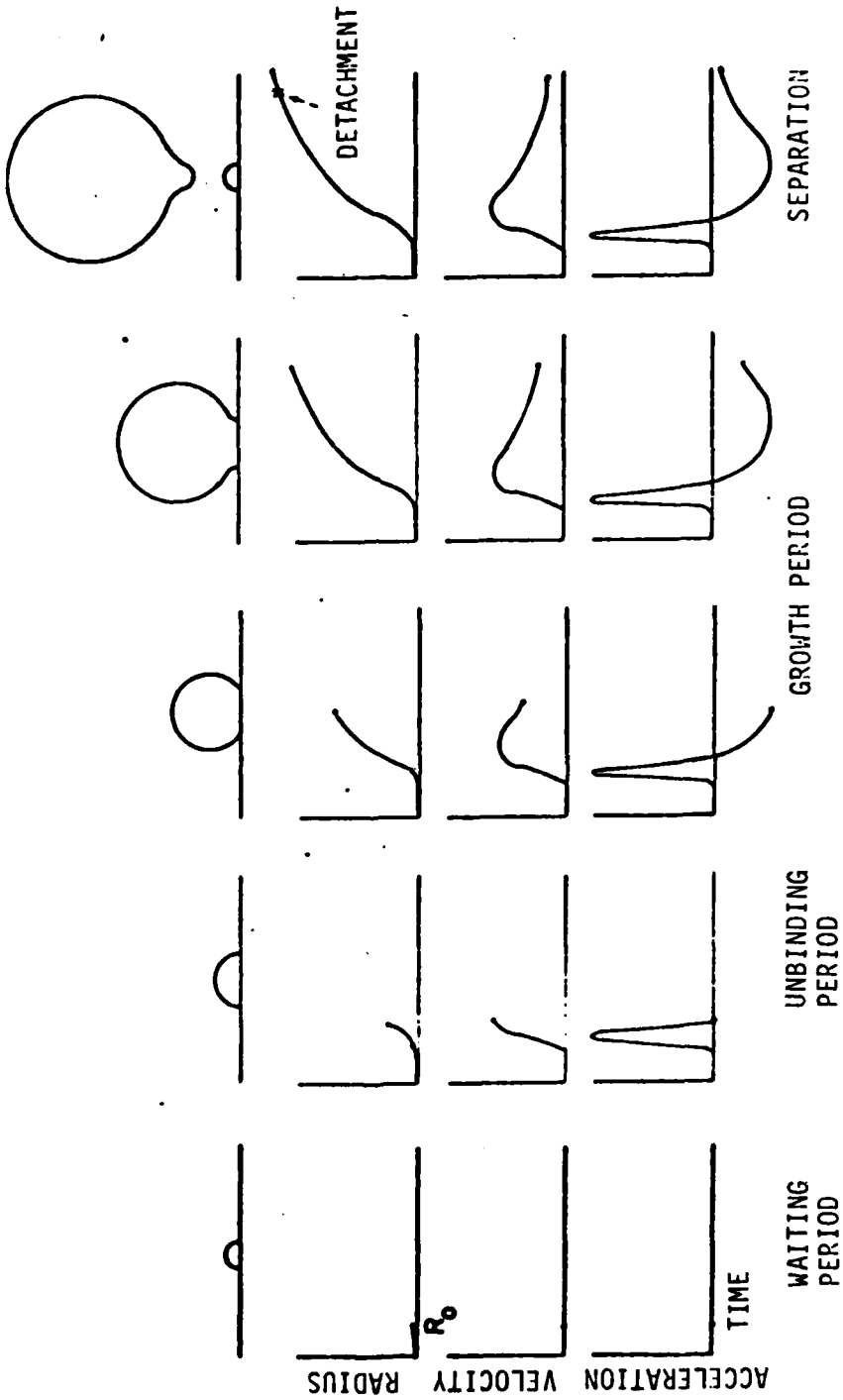

Figure 7. Growth of a Bubble on a Heated Wall

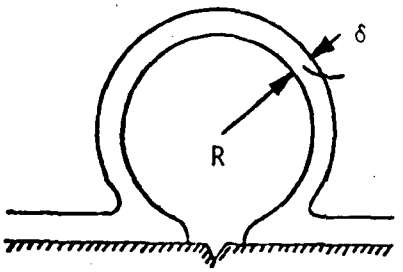

Figure 8. Thermal Boundary Layer Around Growing Bubble

When the bubble departs from the surface it takes the boundary layer with it. Cooler fluid then replaces it on the surface starting the cycle over again. The increased heat transfer rate is caused by hot fluid next to the wall being carried off in this manner and by the fact that only a thin boundary layer is allowed to form creating a larger temperature gradient.

The equation for bubble growth in a uniformly superheated fluid (Equation 4) can be used for the case of a heated wall under low gravity conditions (no natural convection currents) with a few modifications. First, R_o should be replaced by R_{fc} which is the radius corresponding to an imperfection on the surface that is the most favorable for bubble nucleation. Han and Griffith (Reference 9) have analytically derived this most favorable cavity to be:

$$R_{fc} = \frac{4T_{sat}\,\sigma}{(T_w - T_{sat})\,\rho_v L} = 2R_o \qquad (5)$$

Secondly, the fact that the bubble is growing through a temperature gradient must be taken into account. Since convection is negligible, the equation for heat conduction into a semi-infinite solid can be used to determine the temperature distribution in the boundary layer. This equation is:

$$T - T_\infty = (T_w - T_\infty)\,\mathrm{erfc}\left(\frac{x}{2\sqrt{\alpha t}}\right) \qquad (6)$$

where x is the distance from the boundary to the point of interest. The length of time necessary for the boundary layer to grow before bubble growth can begin, derived by Han and Griffith, is:

$$t_w = \frac{144(T_w - T_\infty)^2 \, Tsat^2 \, \sigma^2}{\pi \alpha \rho_v^2 L^2 (T_w - T_{sat})^4} \tag{7}$$

Therefore, with the use of Equations 6 and 7, the initial temperature distribution can be calculated. If one assumes that the temperature of the bubble is that of the coolest spot on the bubble wall, the initial temperature of the bubble is that where x_R equals R_{fc}.

When the bubble starts to grow rapidly it carries the thermal boundary layer with it. As the boundary is carried outward it is thinned by evaporation. Therefore, to calculate the temperature of the bubble as it is growing, the initial temperature profile of the boundary layer is used but the distance at which the bubble temperature is calculated (δ) is modified. The equation for this calculation is found by considering the effects of the change in density during evaporation and curvature effects. As a bubble grows on a surface, the distance from the surface

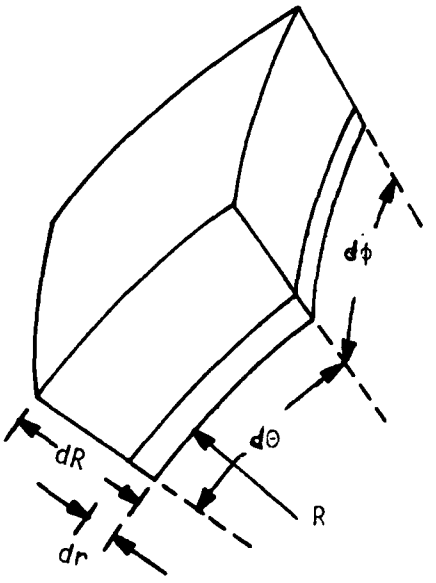

Figure 9. Differential Volume Element

is D, the diameter of the bubble. The effect of the change in density can be derived using the geometry of Figure 9. This figure shows a section of a bubble which has increased in radius by dR. with the final liquid/vapor interface being at R +dR. Since the mass of the increased vapor is equal to the mass of the evaporated liquid:

$$\rho_v dR(Rd\phi)(Rd\theta) = \rho_\ell\, dr(Rd\phi)\,(Rd\theta)$$

or

$$dr = dR\,\frac{\rho_v}{\rho_\ell}$$

Since the distance away from the wall is equal to the diameter, the distance into the boundary layer that is evaporated is 2r.

The curvature effects can be estimated by using potential flow theory and the fluid flow analogy. From the fluid flow analogy, a potential line in fluid flow is equivalent to an isothermal line in heat conduction. Therefore, the distance to the coolest spot of the bubble is πR.

Combining the two effects (boundary layer evaporation and curvature) and starting from R_{fc}, the temperature of the bubble wall can be calculated fromn Equations 6 and 7 using x equal to $R_{fc} + \delta$ where:

$$\delta = \pi R\,(\frac{\rho_v}{\rho_\ell}) \qquad (8)$$

Therefore, the radius at any time can be calculated by solving Equations 4, 5, 6, 7, and 8. The growth of a vapor bubble for saturated water with a wall temperature of 379.2^{o}K has been calculated and is shown in Figure 10, along with experimental data by Keshock and Siegal (Reference 10). As can be seen, the calculated growth rate matches the experimental data quite well.

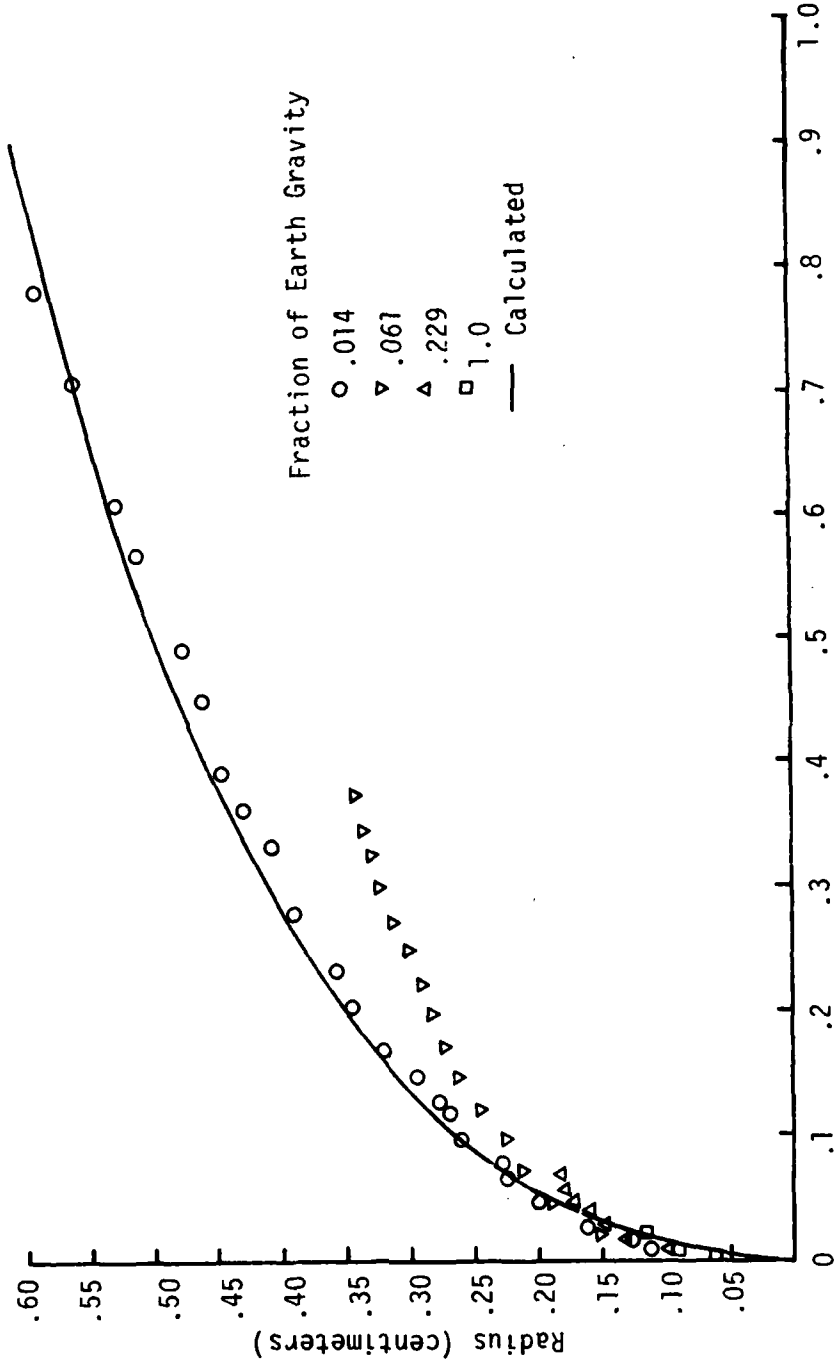

Figure 10. Growth of a Vapor Bubble in Saturated Water with a Wall Temperature of 379.2°K

2. DYNAMICS OF BUBBLE DEPARTURE

Now that we understand how a bubble grows, we need to know why it detaches from the surface in order to get a full understanding of the boiling phenomena. For our purposes, we are especially interested in how gravity affects this process. The following text derives the forces that hold the bubble to the wall and those that pull the bubble away from the wall. Thus, by using a force balance, an estimate of the radius of departure is calculated and compared with experimental measurements for several gravitational accelerations.

a. Forces Acting on a Bubble During Pool Boiling

When the bubble is very small during nucleate pool boiling, the forces that hold the bubble to the wall (negative) are larger than the forces that pull the bubble from the wall (positive). As the bubble grows, the positive forces grow faster than the negative forces until the total force becomes positive (away from the surface). The forces that act on a bubble and their direction can be seen in Figure 11. The negative forces are surface tension and form drag. The positive forces are buoyancy (for an upward facting surface), internal pressure, and inertia. These forces are explained and derived in the following paragraphs.

Surface Tension: This force is caused by the attaction of the liquid to the surface. It acts around the perimeter of the bubble base and is proportional to the surface tension of the fluid times the sine of the angle of the wedge of liquid between the surface and the bubble wall, or:

$$F_S = \pi D_b \sigma \sin\theta$$

where D_b is the base diameter.

As the bubble nears departure, the base begins to neck down causing θ to go to 90^o. Therefore, at departure:

$$F_S = \pi D_b \sigma \qquad (9)$$

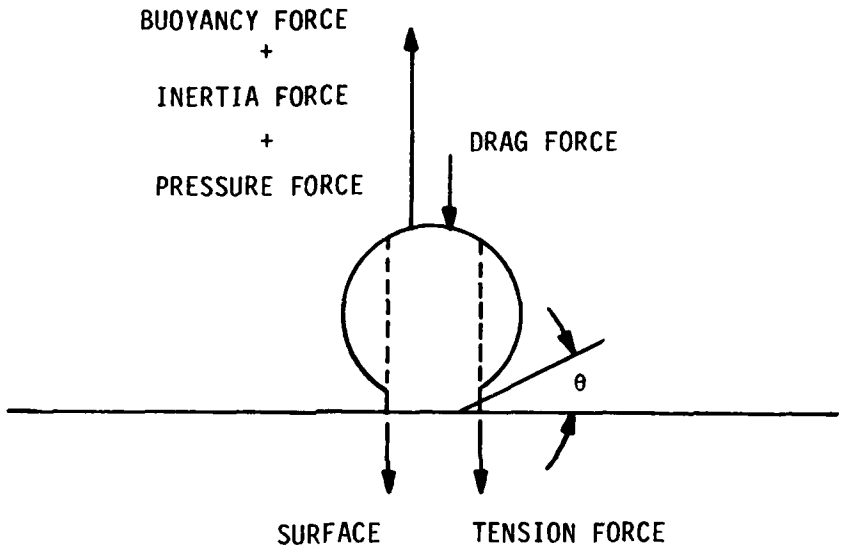

Figure 11. Forces Acting on a Vapor Bubble

Drag: This force is caused by the fact that the bubble grows in a viscous fluid. In many cases, this force is negligible. However, a rough estimate of this force was made by Keshock and Siegel (Reference 10) and is used here. It is assumed that the bubble is spherical and growing away from the wall at a velocity equal to the change of its diameter with time. The drag coefficient used was $C_D = 45/_{Re}$ where:

$$Re = \frac{\rho_\ell D}{2\mu_\ell} \frac{dD}{dt}$$

The drag force is:

$$F_D = 1/2\ \rho_\ell\ C_D\ \frac{\pi D^2}{4}\ (1/2\ \frac{dD}{dt})^2$$

or:

$$F_D = \frac{45\pi}{16}\ \mu_\ell\ D\ \frac{dD}{dt} \qquad (10)$$

Buoyancy: The buoyancy force depends on Archimedes principle which states "a body submerged in a stagnant fluid is subject to a force equal to the weight of the fluid it displaces." For a spherical bubble:

$$F_B = \frac{\pi D^3}{6}\ (\rho_\ell - \rho_v)g \qquad (11)$$

Historically, this was the only force considered to cause bubble departure from a heated surface in pool boiling. As a result, it was reasoned that, as the gravitational acceleration is reduced, the force of buoyancy goes to zero, and nucleate boiling cannot occur. It has been discovered, however, that in many circumstances, nucleate boiling does occur under zero-gravity conditions. In fact, with certain fluids, nucleate boiling behavior shows little dependence on gravity (Reference 10). This may occur because the following two forces are independent of gravity and also work to separate the bubble from the surface.

Internal Pressure: For a bubble completely surrounded by liquid, the net force due to internal pressure is zero. When the bubble is attached to a surface, however, this pressure force is unbalanced over the attached base area. The pressure difference between the inside and outside of a spherical bubble of radius R is:

$$P_i - P_o = \frac{2\sigma}{R}$$

The force exerted is:

$$F_P = \frac{2\sigma}{R} \pi R_b^2 \qquad (12)$$

where R_b is the radius of the base. It should be noted that this force is maximum when the bubble is a hemisphere. At this point, the force is equal and opposite to the surface tension force. Therefore, this force alone cannot separate a bubble from the surface.

Inertia: This force has been widely misunderstood in the past. It is known that the inertia of the vapor plays a small role in the growth of a bubble. This vapor inertia is an extremely small force in nucleate boiling and can be completely ignored after the very short unbinding period (Reference 9). This small role of the vapor inertia has caused most investigators in the past to neglect the effect of inertia on bubble departure.

Although the vapor inertia is negligible during most of the growth of a bubble, *the inertia of the liquid surrounding the bubble is not.* As the bubble grows, the liquid surrounding the bubble is put into motion. According to Han and Griffith (Reference 9), the apparent mass of the affected fluid is that occupied by 11/16 of the bubble volume. After the initial unbinding period, the growth rate of the bubble begins to decrease. The interia of the liquid opposes this decrease in velocity, thus attempting to pull the vapor with it. This inertia force, therefore, tends to pull the bubble away from the surface. From Newton's 2nd law:

$$F_I = \frac{d}{dt} (mu) = \rho V \frac{du}{dt} + \rho u \frac{dV}{dt}$$

where V is the volume and u is the velocity. Since a bubble on a surface can only grow outward, the velocity is equal to the change of diameter with time, or

$$F_I = \rho V \frac{d^2D}{dt^2} + \rho \frac{dD}{dt} \frac{dV}{dt}$$

Using 11/16 of the bubble volume:

$$F_I = \frac{11}{96} \pi \rho_\ell \left(D^3 \frac{d^2D}{dt^2} + 3D^2 \left(\frac{dDm}{dt}\right) \left(\frac{dD}{dt}\right)\right.$$

The term $\frac{dDm}{dt}$ is the velocity at which the differential mass element departs from the bubble wall. For a rocket, this velocity is equal to the exhaust velocity of the engine. In evaporation at a bubble wall, however, a differential mass element does not depart. Instead, it stays immediately adjacent to the bubble wall. Therefore, dDm/dt equals zero and the force of inertia can be written as:

$$F_I = \frac{11}{96} \pi \rho_\ell D^3 \frac{d^2D}{dt^2} \tag{13}$$

b. Calculation of Departure Radius for Pool Boiling

The departure radius was assumed to be the radius at which the total force went from negative to positive. This calculation was carried out using Equations 9 through 13 for saturated water boiling under 1-g, 0.229-g, and 0.061-g accelerations on a wall heated to 379.2°K. The data used to calculate the forces was taken from a paper by Keshock and Siegel (Reference 10), and the results are presented in Figure 12 with "best fit" curves. The forces acting on a bubble versus the radius of the bubble are shown in Figures 13 through 15.

For 1-g, the actual radius of departure (Reference 11) was .118 cm while the calculated value was .115 cm or an error of 2.5%. For 0.229-g, the actual radius (Reference 10) was 0.179 cm while the calculated value was 0.174 cm, or a 2.8% error (Reference 10). For 0.061-g, the actual radius (Reference 10) of departure was 0.342 cm where the calculated value was 0.340 cm, or a .6% error. It should be noted, however, that for 0.061-g, the bubble base radius decreased rapidly prior to detachment. The force balance before this necking down occurred was still negative which indicates that another force caused the necking down to occur. This force is thought to be interference from other bubbles since the bubbles grow to relatively large diameters under low gravity conditions.

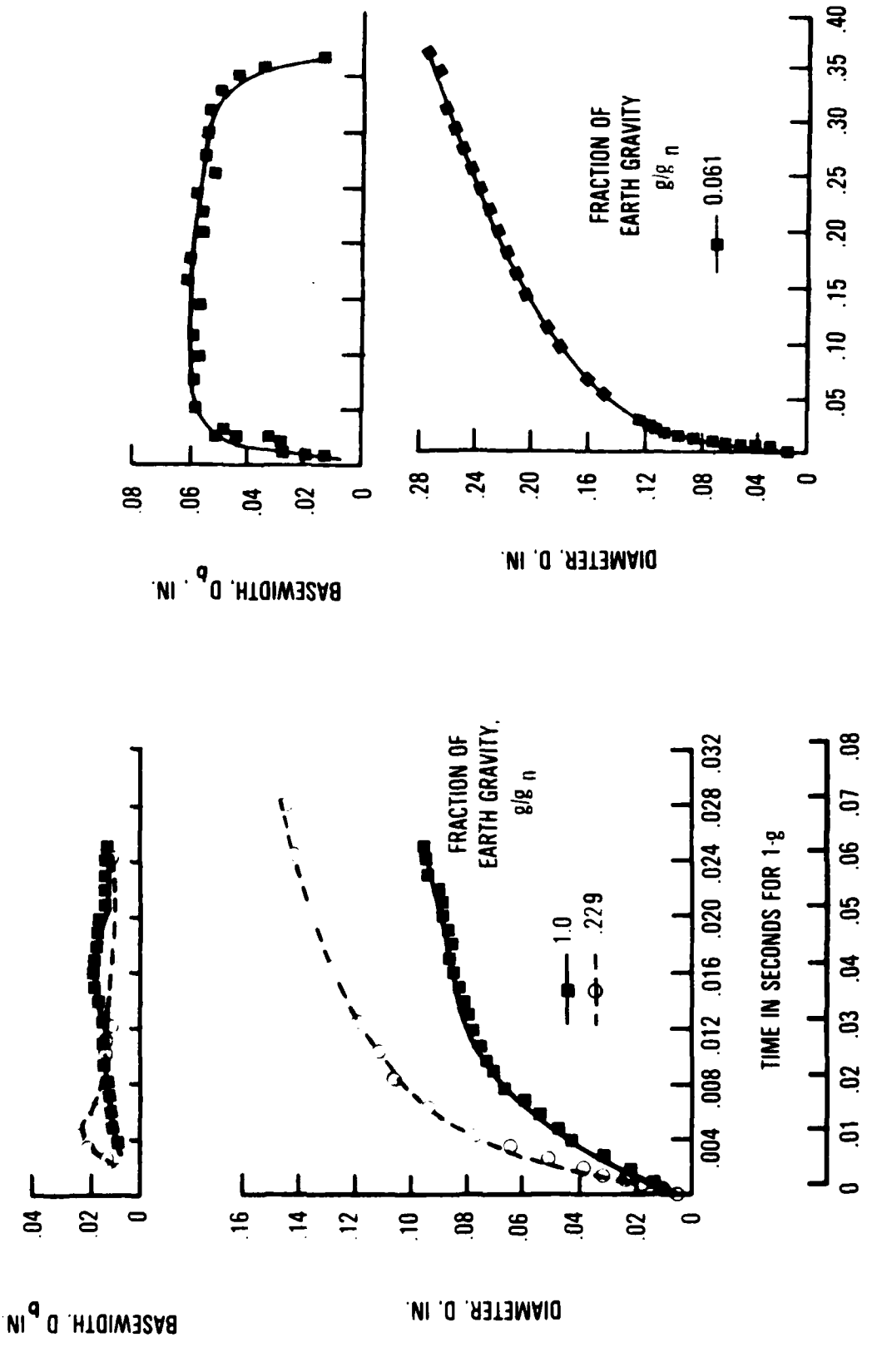

Figure 12. Growth of Vapor Bubbles in Saturated Water on a 179.2°K Wall

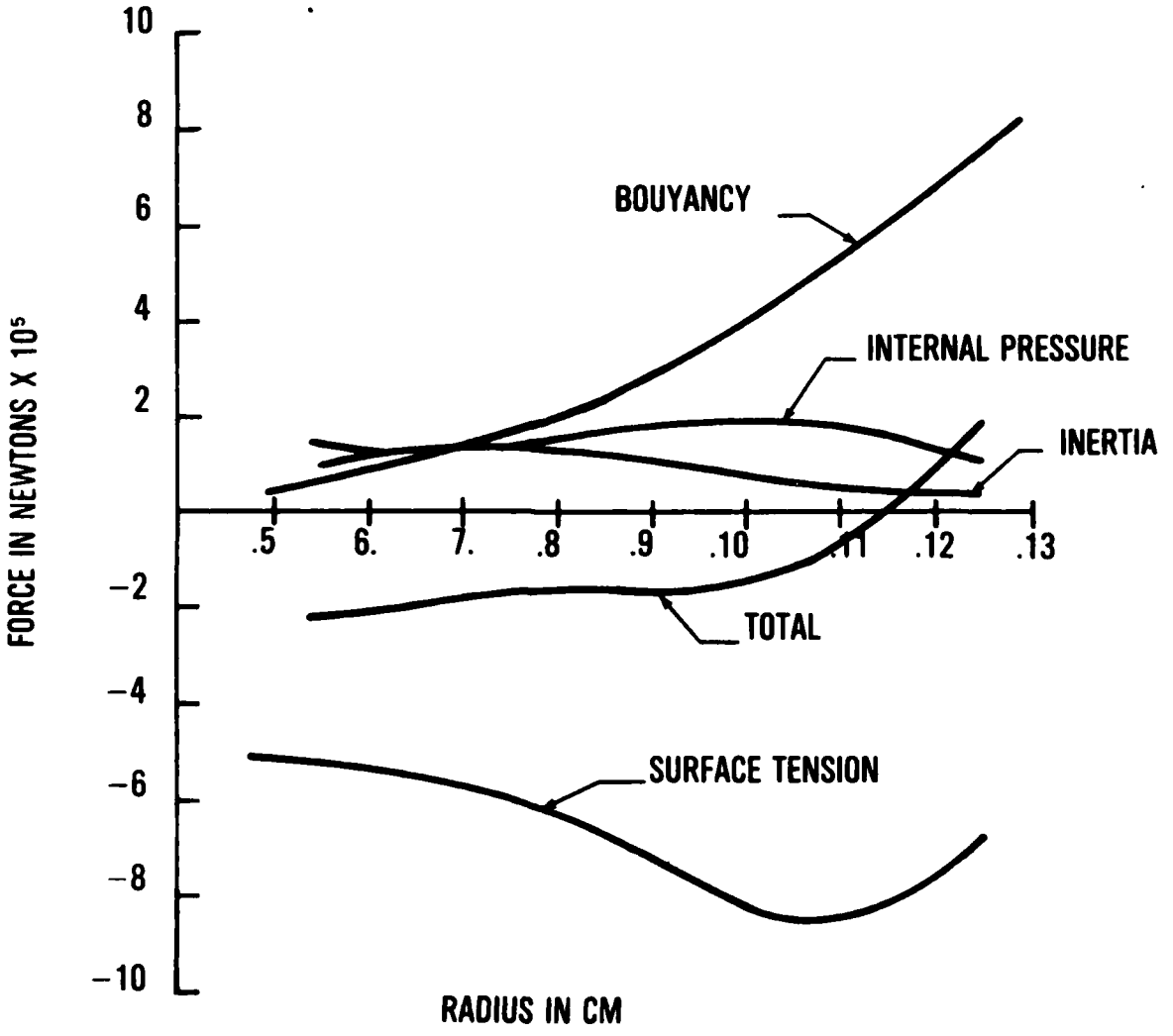

Figure 13. Forces Acting on a Bubble in Saturated Water on a 379.6°K Wall Under 1-g Acceleration

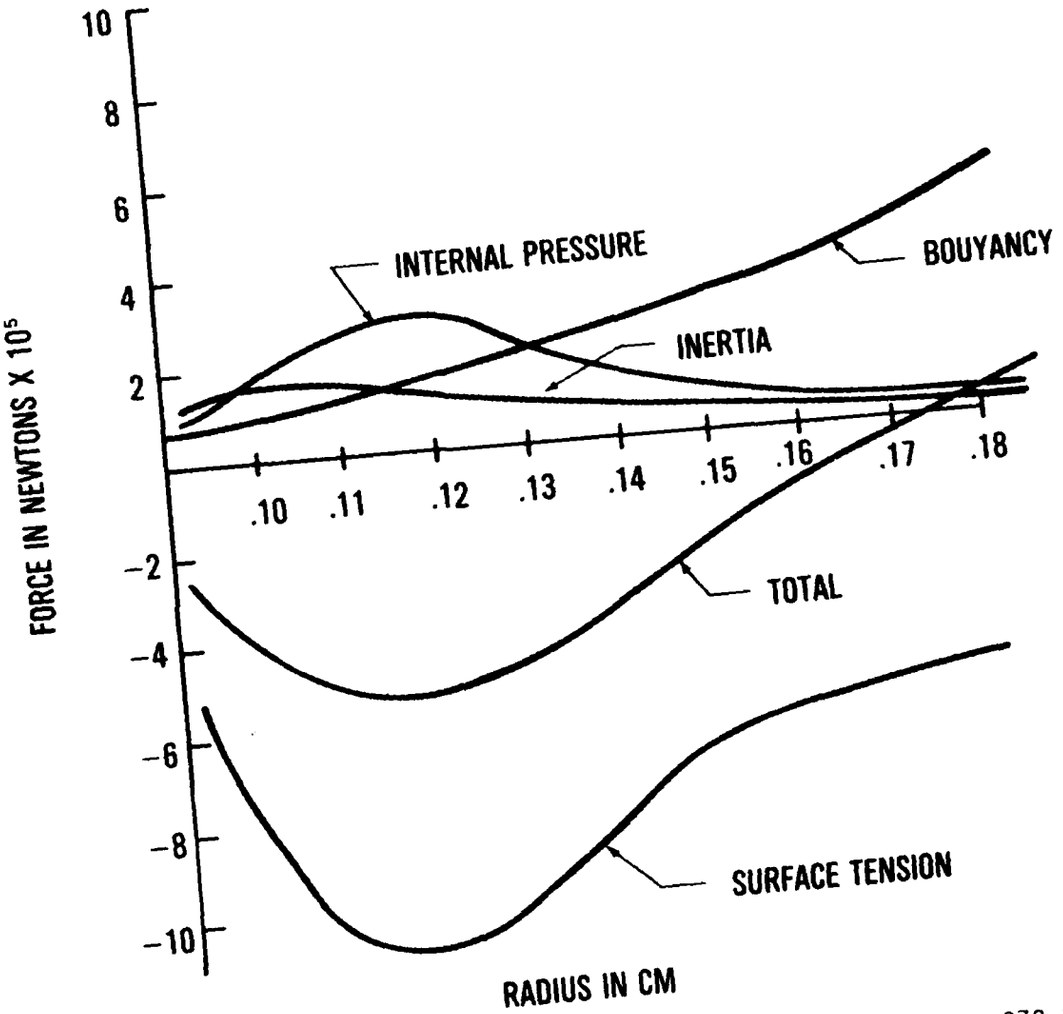

Figure 14. Forces Acting on a Bubble in Saturated Water on a 379.2°K Wall Under .229-g Acceleration

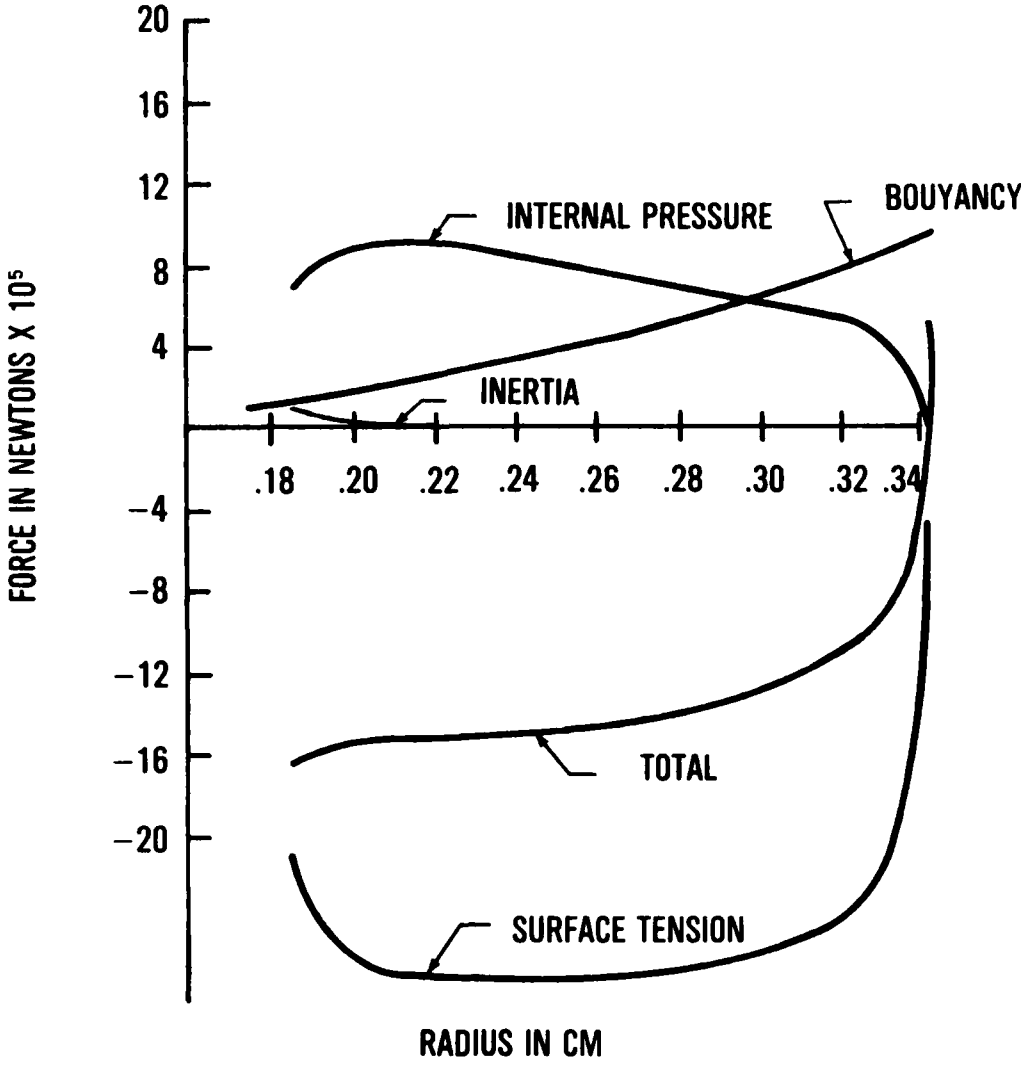

Figure 15. Forces Acting on a Bubble in Saturated Water on a 379.2°K Wall Under .061-g Acceleration

It should also be noted that steam bubbles growing on a 379.2°K wall under 0-g conditions and with no interference from other bubbles will not detach from the surface. However, for other fluids or for water under different conditions, nucleate boiling may work under 0-g conditions. As mentioned before, Keshock and Siegel (Reference 10) found that detachment diameters were relatively independent of gravity for aqueous-sucrose solutions. This is caused by the inertia force dominating the buoyancy force for these fluids. Therefore, anything that increases the inertia force such as subcooling of the bulk fluid or increasing the wall temperature (which increases the initial growth rate and increases the deacceleration) will decrease the dependence of nucleate pool boiling on gravity. (The drag force in all of these calculations was found to be negligible.)

c. Forces Acting on a Bubble During Forced Convective Boiling

All of the preceding forces which act to separate a bubble are present during forced convection as well as one additional force. This force is the form drag of the bubble caused when a viscous fluid flows parallel to the wall. These forces can be seen in Figure 16. The drag force tends to shear the bubble off the surface. However, no attempt has been made here to determine its magnitude when compared to the previously mentioned forces. The macroscopic aspects of forced convection boiling are reviewed in the next subsection.

3. FORCED CONVECTION BOILING

a. General Considerations

Consider forced convection flow with a liquid entering a heated tube. At some place along the tube the liquid reaches the saturation temperature, and local or nucleate boiling takes place. In this region (Region 1), the vapor formation occurs at the heated surface in the form of bubbles that grow, detach and become dispersed in the flowing liquid. The flow can be considered as bubbly flow when the quality range is flowing from approximately 5 to 10%. The heat transfer coefficient in this region is practically constant.

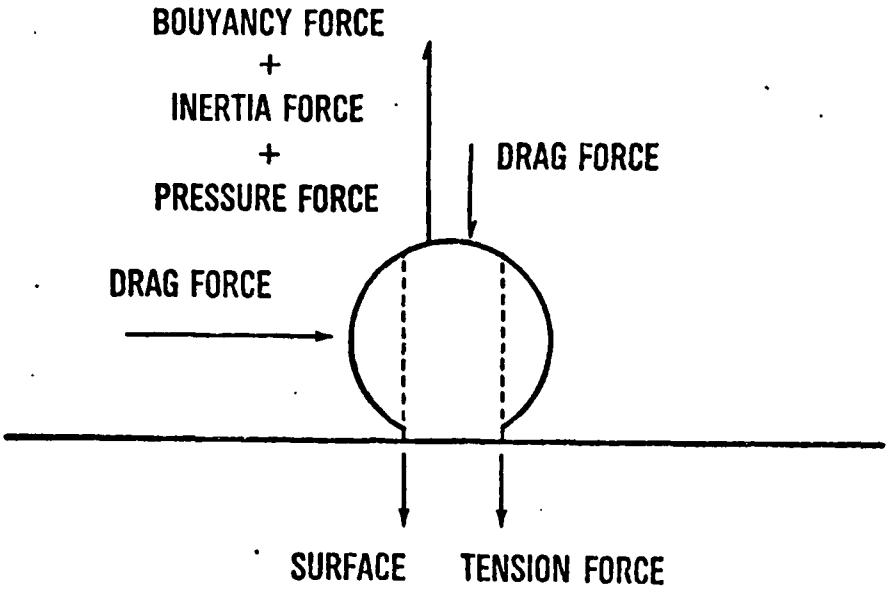

Figure 16. Forces Acting on a Vapor Bubble in Forced Convective Boiling

At higher qualities (Region 2) the flow becomes annular with a vapor core which may or may not contain significant amounts of liquid droplets. If the liquid film on the wall is thin enough, heat is transferred by conduction through the liquid and vaporization occurs at the liquid-vapor interface. Under these conditions, the wall temperature is below that required for nucleation or activation of the cavities. At higher heat fluxes, nucleation will take place under the liquid layer at the wall. In this region the heat transfer coefficient increases with quality because of the increased flow velocity.

At some point down the channel the heated wall may become dry (Region 3). Beyond this point, the wall temperature usually rises significantly for a particular heat flux. In this liquid deficient region, the heat transfer coefficient decreases with increased quality.

Figure 17 presents the different boiling regimes along a heated channel.

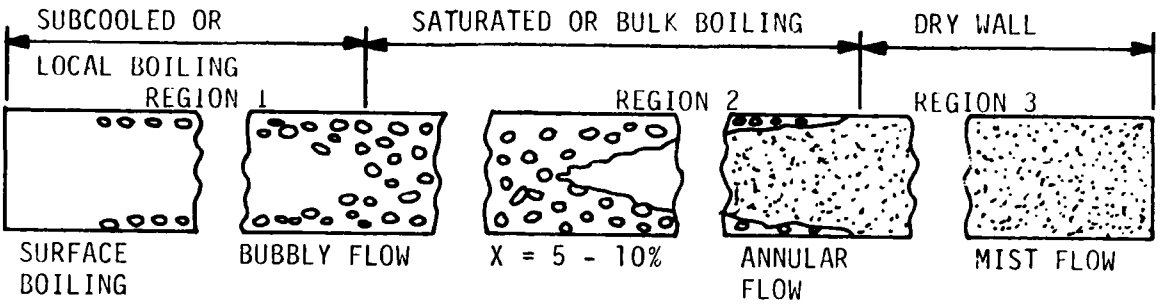

Figure 17. Boiling Regimes

Review of numerous analytical and experimental studies performed by many investigators indicates that a general correlation of convective boiling data does not seem possible because of the strong influence of minor variables which are difficult if not impossible to control. Among these variables are the amounts of dissolved and adsorbed gases and impurities in the fluid, including contamination and finish of the surface. All these variables have a pronounced effect on both the slope and position of the boiling curve.

Attempts, however, have been made to develop some empirical expressions for predicting boiling heat fluxes using the method of superposition. Bergles and Rohsenow (Reference 12) presented a convective boiling heat flux $(Q/A)_c$ expression for water over a pressure range of 15 to 2000 psia.

$$(Q/A)_i = 15.00\ p^{1.156}\ (T_w - T_{sat})^{2.3}/p^{0.0234} \qquad (14)$$

where T_w is the wall temperature and T_s is the fluid saturation temperature.

The above incipient boiling equation has been found valid for several commercially finished surfaces which can be expected to have a wide range of cavity sizes. Similar expressions may be developed for other fluids. Although velocity does not appear in the equation, it seems valid for all fluid velocities.

In the region of strong nucleate boiling for both pool and forced convection surface boiling, the test data of many investigators can be expressed as follows:

$$(Q/A)_B = C(T_w - T_{sat})^n$$

where the constant C and the exponent n depend upon the particular fluid and surface conditions (for most surfaces n≈4).

Reference 12 points out that, in accordance with water tests, the sequence of wall temperature variation with heat flux was reproducible with the transition always starting at about 15°F of wall superheat. For 38 psia and Q/A = 0.45 x 10^6 BTU/hr. ft^2, the incipient boiling analysis predicts the start of boiling at $(t_w - t_s)$ = 17.5°F.

Experimental data for forced convection boiling inside ducts or across wires and plates can be presented as shown in Figure 18.

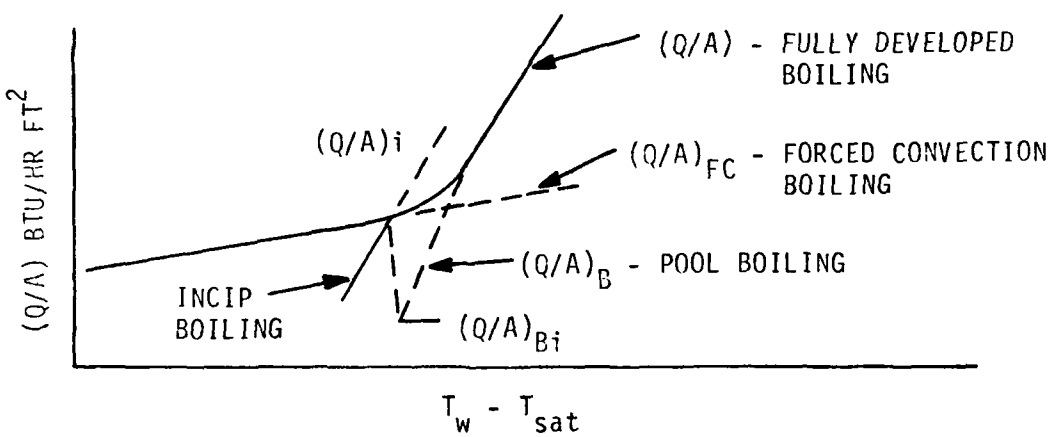

Figure 18. Forced Convection Surface Boiling

As the heat flow to a saturated liquid is increased beyond the incipient boiling point, the number of spots on the surface from which bubble columns rise increases. Reference 2 proposes the following three equations for subcooled and low-quality (up to 10%) forced convection boiling of water:

$$\text{Jens and Lottes:} \quad T_w - T_{sat} = \frac{60}{e^{p/900}} \left(\frac{Q''}{10^6}\right)^{1/4} \tag{16}$$

$$\text{Weatherhead:} \quad T_w - T_{sat} = (90 - 0.127\, t_s) \left(\frac{Q''}{10^6}\right)^{1/4} \tag{17}$$

$$\text{Thom:} \quad T_w - T_{sat} = e^{\left(\frac{72}{P/1260}\right)} \left(\frac{Q''}{10^6}\right)^{1/2} \tag{18}$$

where $Q'' = Q/A$, BTU/hr. ft^2, P = pressure, psia

At vapor qualities above 10%, the boiling regime is considered as high quality forced convection boiling. Various investigators have suggested a variety of correlation equations for this boiling regime which are presented in Reference 13. The Chen equation is recommended for the lower quality region, while the Dengler and Addoms equations are suggested for the higher quality regions.

The Chen Equation (Reference 18)

$$h = 0.00122 \left[\frac{k_\ell^{0.79} C_{p\ell}^{0.45} \rho_\ell^{0.49} g_c^{0.25}}{\delta^{0.5} \mu_\ell^{0.29} L^{0.24} \rho_v^{0.24}}\right] \left[(\Delta T)^{0.24} (\Delta P)^{0.75} + S + h_{LP} F\right] \tag{19}$$

with $\Delta P = \frac{\Delta TL}{T_{sat}\, v_v}$, difference in saturation pressure corrected to $\Delta T = T_w - T_{sat}$.

S and F are given in Figures 19 and 20; h_{LP} = heat transfer coefficient for liquid phase alone flowing in the tube,

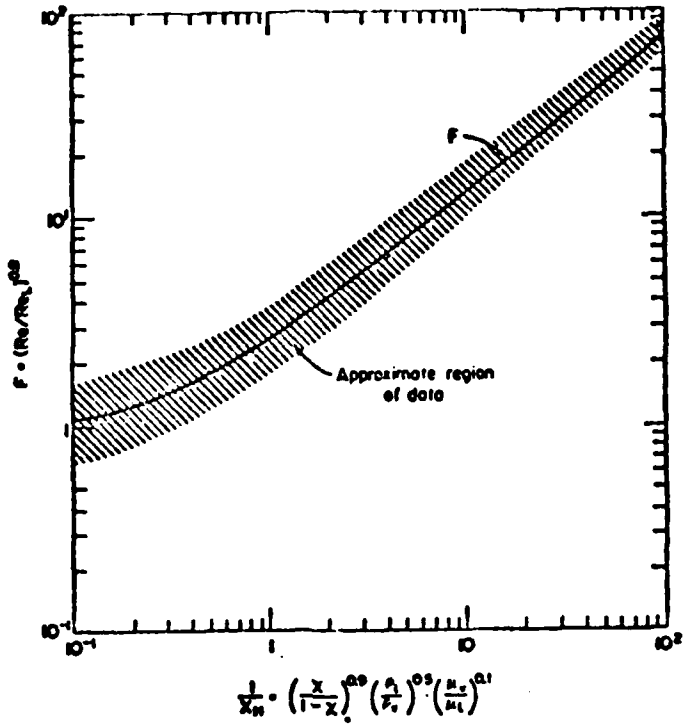

Figure 19. Reynolds Number Factor F

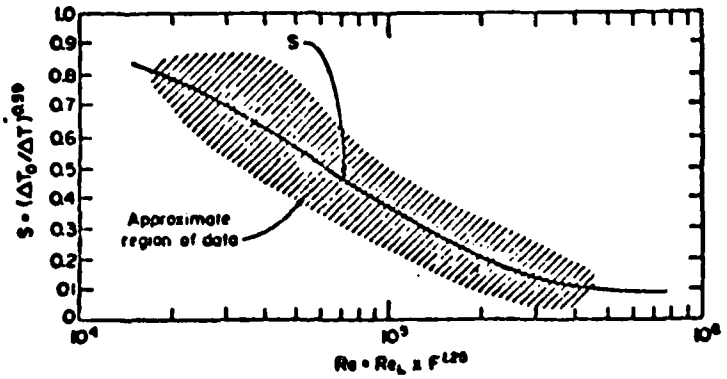

Factor 20. Suppression Factor S

Dengler and Addoms Equation (Reference 19)

$$\frac{h}{h_{LO}} = 3.5 \left(\frac{1}{X_{tt}}\right)^{0.5} \tag{20}$$

where $\frac{1}{X_{tt}} = \left(\frac{x}{1-x}\right)^{0.9} \left(\frac{\mu_v}{\mu_\ell}\right)^{0.5} \left(\frac{\mu_v}{\mu_L}\right)^{0.1}$, Martinelli parameter

for convective region only: $0.25 < X_{tt} < 70$

To take into account nucleation, multiply by F

h_{LO} = heat transfer coefficient when all liquid flowing in tube

$$h_{LO} = 0.023 \frac{k_L}{D} \left(\frac{GD}{\mu_L}\right)^{0.8} Pr_L^{0.4}$$

$$h_{LP} = 0.023 \frac{k_L}{D} \left[\frac{G(1-x)D}{\mu_L}\right]^{0.8} Pr_L^{0.4}$$

The above equation has been correlated for water within $\pm$ 20 percent.

Pierre equation

$$N_u = C \left[(Re_{LO})^2 (K_f)^{0.5}\right]^{\nu} \tag{21}$$

where C and ν are numbers defined in Reference 13.

for x_{in} = 0 to 0.56

x_{out} = 0.08 to 1.0

$(Re_{LO})^2(K_f) = 10^9$ to 0.7×10^{12}

C = 0.0009, ν = 0.5

for $x_{in} < 0.5$

x_{out} = 1.0 to 11°F superheat

$(R_{e_{Lo}})^2 (K_f) = 10^9$ to 0.7×10^{12}

$C = 0.0082$, $\nu = 0.4$

$$K_f = \frac{J\Delta x\ L}{\Delta_\ell}$$

$$Re_{Lo} = \frac{GD}{\mu_L}; \quad Re_{Lp} = \frac{G(1 - x)\ D}{\mu_L}$$

$$Nu = \frac{hD}{k\ell}$$

The above equation has been correlated for R-11, R-12 and R-22 within --10% and +20%. It is valid for the average heat transfer coefficient h along the tube.

b. Critical Heat Flux

Test data in the vicinity of burnout can be divided into four general regions as shown in Figure 21 (from Reference 13). Beyond a critical heat flux, the surface temperature begins to rise sharply and to oscillate until the wall is completely dry and film boiling takes place. The critical heat flux is associated with a sharp reduction in the ability to transfer heat from the surface.

A complete description of flow phenomena leading to burnout is given in Figure 21. In Region I, no boiling takes place, and it can be considered as single-phase forced convection. Region II is characterized by an increased heat transfer coefficient because of the increased vapor generation rates and flow velocity. As the quality increases down the channel, the vapor velocity may become large enough to tear the liquid off the wall, resulting in the temperature oscillation associated with Region III. At sufficiently high heat flux, the wall could become dry causing a fog flow or film boiling where a vapor film separates liquid from the wall, Region IV. Under certain flow rate and heat flux

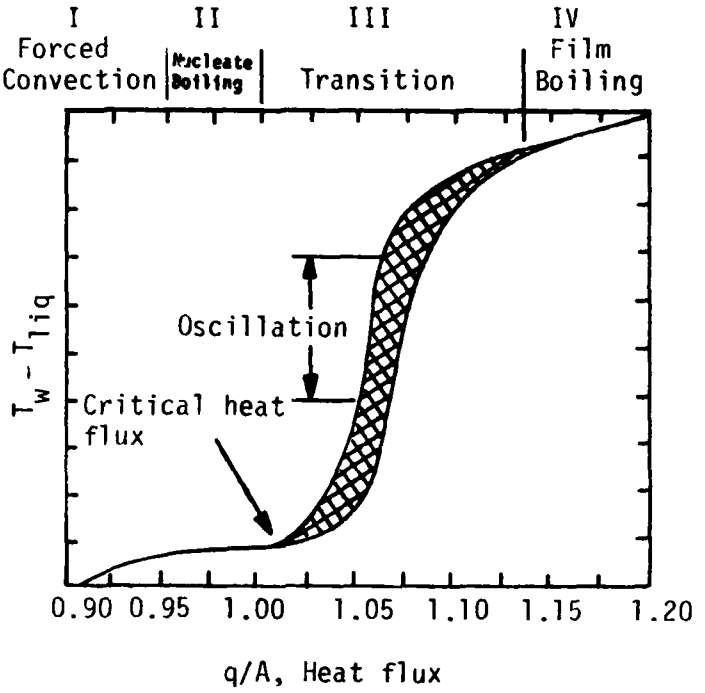

Figure 21. Typical Temperature History During Burnout

conditions, the wall temperature can reach the melting point of the material resulting in burnout.

System oscillations can be reduced or even eliminated by placing orifices ahead of the boiler. The damping effects can be further improved by placing several orifices in series. It has been observed from experiments that the critical heat flux $(Q/A)_{crit}$ of an unstable system is significantly lower than the experienced under stable flow conditions. It has also been observed that the onset of flow oscillations in forced flow subcooled boiling is a strong function of inlet subcooling and system pressure. An increase in inlet subcooling or a decrease in system pressure tends to induce subcooled boiling oscillation.

Correlation of Critical Heat Flux

For subcooled liquid Gambill, (Reference 14) has developed the following expression:

$$(Q/A)_{crit} = (Q/A)_{b,crit} + (Q/A)_{c,\,crit} \tag{22}$$

where: $$(Q/A)_{b,crit} = 0.145L\,\rho_v\left[\frac{\sigma\, g_c\, g\,(\rho_L - \rho_v)}{\rho_v^2}\right]^{1/4}$$

$$\cdot\left[1 + \left(\frac{\rho_L}{\rho_v}\right)^{0.923}\left(\frac{C_{PR}\,\Delta T_{sub}}{25L}\right)\right]$$

$$(Q/A)_{c,crit} = h_c(T_{w,crit} - T_{liq})$$

$T_{w,crit}$ is evaluated from Bernath's relation (Reference 15)

$$T_{w,crit} = 102\ \ln P - 97\left(\frac{P}{P+15}\right) - \frac{u}{2.22} + 32 \tag{23}$$

where P is absolute pressure in psia, and u is flow velocity in ft/sec assuming all liquid flow. h_c is the heat transfer coefficient assuming all liquid flow in the channel.

Other empirical correlations have been developed and can be found in published literature. The correlation attempts, however, have been made for water only. The $g^{1/4}$ variation for $(Q/A)b_{crit}$ is only a lower limit.

Miscellaneous Effects

Some test results have indicated that an increase of approximately 20% in $(Q/A)_{crit}$ was achieved when roughness was increased from 20 to 200 micro-inches. In contrast to results for pool boiling, the effect of dissolved gas in flow boiling $(Q/A)_{crit}$ has been found to be insignificant.

As means of delaying the film dryout, twisted ribbons or tapes in tubes and vortex flow at the inlet have produced increases in $(Q/A)_{crit}$.

4. BOILING PROCESS SUMMARY

The high heat transfer rates achievable during nucleate boiling are caused by the fact that the thermal boundary layer that forms on the wall is carried outward by the bubbles. This not only directly transports energy away from the surface, but also allows cooler fluid to reach the wall, thus creating a larger temperature gradient.

The nucleate boiling process is controlled by five forces during pool boiling and six during forced convection. In pool boiling, surface tension and form drag hold the bubble to the surface while buoyancy, internal pressure, and liquid inertia tend to separate it from the surface. For most liquids, the drag force can be ignored. The buoyancy force is directly related to the local gravitational acceleration while the inertia force is independent of gravitational acceleration but is directly proportional to the acceleration of the bubble wall. The magnitude of the buoyancy force, when compared to the inertia force, will indicate the relative dependence of nucleate pool boiling on gravity. Therefore, the larger the inertia force, the more independent of gravity the nucleate pool boiling phenomena becomes.

Under forced convection conditions there is another drag force caused by the viscous liquid flowing past the bubble and parallel to the wall. This force shears the bubble at the wall.

During forced convection, the boiling process can be broken down into three regions: bubbly flow, annular flow, and mist flow. The flow region encountered locally must be known before a calculation of the local heat transfer coefficient can be made. The following is a summary of the recommended equations for calculating the heat transfer coefficient.

In the subcooled liquid, Stag, Dengler, and Addoms (Reference 13) obtained the correlation:

$$h = 0.023 \left(\frac{k}{D}\right) (Re)^{0.8} (Pr)^{0.4} \quad \text{(turbulent flow)}$$

For the bubbly flow region the following empirical equation (Reference 16) has been found useful for a number of organic liquids:

$$\frac{hD}{k_\ell} = c \left[\frac{Q''D}{ML}\right]^{0.69} \left[\frac{c_{p\ell}\mu}{k_\ell}\right]^{0.69} \left[\frac{\rho_\ell}{\ell_v} - 1\right]^{0.31} \left[\frac{PD}{\sigma}\right]^{0.31}$$

The constant c = .225 for a plain tube.

For water, Jakob (Reference 17) presents the following equation

$$Nu = 0.028\ (Re)^{0.8}\ (Pr)^{0.4}$$

with a range of quality of x = .25 to 4% and a range of flow velocity of u = 2.4 to 15 ft/s.

For annular flow, Lavin and Young (Reference 16) give the following:

$$h_{LP} = 0.023\ \frac{k_\ell}{D} \left[\frac{GD(1 - x)}{\mu_\ell}\right]^{0.8} [Pr]^{1/3} \left[\frac{\mu_\ell}{\mu_w}\right]^{0.14}$$

$$\frac{h_{TP}}{h_{LP}} \left[\frac{GL}{Q''}\right]^{0.1} = C_2 \left[\frac{1 + x}{1 - x}\right]^{1.16}$$

$$C_2 = 3.75 \text{ to } 5.0$$

h_{LP} is the heat transfer coefficient of the liquid phase alone, h_{TP} is the heat transfer coefficient of the two-phase mixture, Q is the heat flux, and μ_w is the viscosity at the wall.

For low quality mist flow, Chen (Reference 18) presents the following equation:

$$h = 0.00122\ \frac{k_\ell^{0.79}\ C_{p\ell}^{0.45}\ \rho_\ell^{0.49}\ g_c^{0.25}}{\sigma^{0.5}\ \mu_\ell^{0.29}\ L^{0.24}\ \rho_v^{0.24}} (\Delta T)^{0.24}\ (\Delta P)^{0.75} S + h_{LP} F$$

with

$$\Delta P = \frac{\Delta TL}{T_s \nu_{fg}} \quad \text{and} \quad \Delta T = T_w - T_{sat}$$

S and F where shown previously in Figures 19 and 20.

For high quality vapor, Dengler and Addoms give:

$$\frac{h}{h_{Lo}} = 3.5 \left(\frac{1}{X_{tt}}\right)^{0.5} \quad ; \; 0.25 < x_{tt} < 70$$

where

$$\frac{1}{X_{tt}} = \left(\frac{x}{1-x}\right)^{0.9} \left(\frac{\rho_\ell}{\rho_\nu}\right)^{0.5} \left(\frac{\mu_\nu}{\mu_\ell}\right)^{0.1}$$

h_{LO} is the heat transfer coefficient when all liquid is flowing through the tube.

These equations and their respective region of use are shown in Figure 22.

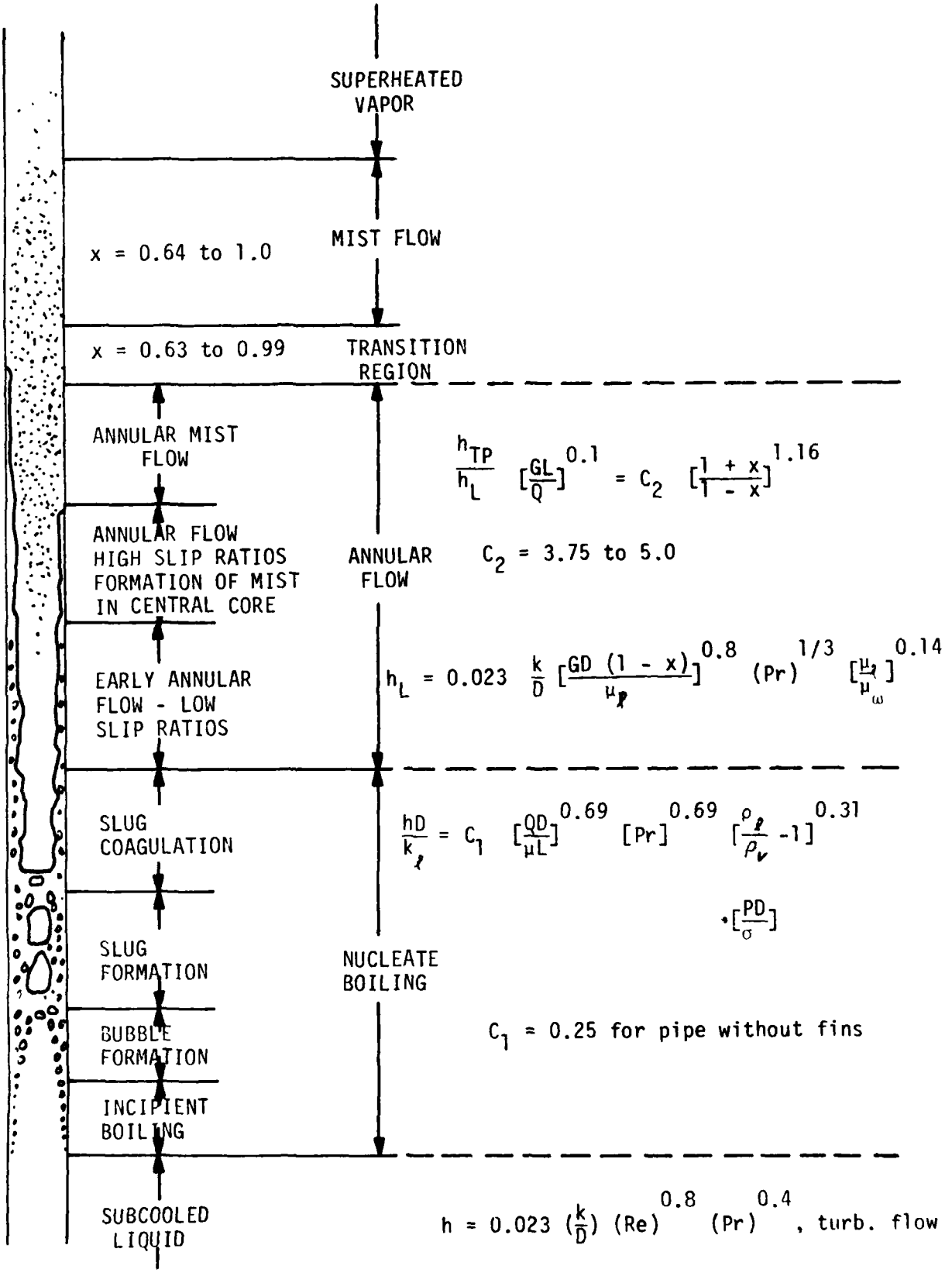

Figure 22. Model of Evaporation Inside a Vertical Tube

SECTION III

CONDENSATION PROCESS

1. BASIC EQUATIONS

Numerous equations and analytical techniques have been developed for predicting condenser performance. Quite different results, however, can be obtained by using these different equations or techniques for the same condenser configuration. It must also be realized that predictions can differ from actual test data within a range of ± 25 percent and even more, depending on the condition and condenser configurations.

At high vapor flow velocities, and particularly during condenser operation in a zero gravity environment, the condensate flow regime becomes annular with a vapor core in the center of the tube. Figure 23 shows such a condensation process.

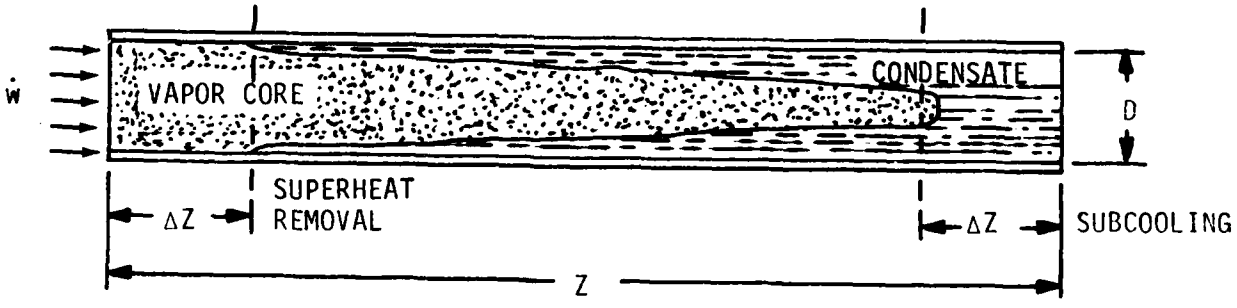

Figure 23. Annular Condensation Process

In the annular film condensation process the heat transfer resistances are divided into two parts. One is the resistance due to interphase mass transfer and the other is the conduction resistance through the condensate film. While the interphase mass transfer resistance is the predominant resistance in the condensation of high thermal conductivity fluids like liquid metals, it is rather small for the condensation of low conductivity material, such as refrigerants. A standard approach for condenser calculations with low thermal conductivity fluids is described below. The overall heat transfer

coefficient, U, may be determined from the following expression (neglecting wall resistance);

$$\frac{1}{U} = \frac{1}{h_z} + \frac{\delta}{k_L} + \frac{1}{h_o} \tag{24}$$

where h_z is the local condensation heat transfer coefficient, watts/m^2.^oC, (Btu/hr.ft^2)

δ is the condensate film thickness, m (ft)

k_L is the thermal conductance of the condensate, w/m^oC (Btu/hr.ft.^oF)

h_o is the external convection or radiation heat transfer coefficient, w/m^2C (Btu/hr.ft.^{2}.^oF)

The heat transfer coefficients should all be based on the same area per unit length of the condenser. If extended surfaces are used on one or both of the heat transfer surfaces, then the area ratios must be included with the particular heat transfer coefficients.

As the flow velocity and quality of the vapor changes along the condenser flow path, it is more convenient to divide the condenser into a number of sections. Based on the quality changes, heat transfer coefficients and condensate film thickness can be determined for each of the sections.

Assuming that vapor enters the condenser in a superheated condition, the superheat must be removed before condensation will take place.

a. Removal of Superheat

Heat removal from a condenser section that is superheated is given by:

$$Q = \dot{w}(h_1 - h_2) \tag{25}$$

where $\dot{w}$ is the vapor flow rate, g/s (lb/hr)

h_1 is the enthalpy of superheat, j/g (Btu/lb)

h_2 is the enthalpy of saturated vapor, j/g (Btu/lb)

The heat rejected to the heat sink is:

$$Q = AU\ (T_v - T_s) \tag{26}$$

where $A = \pi D(\Delta Z)$, heat transfer area, $m^2(ft^2)$

U is the overall heat transfer coefficient, $w/m^2\ ^oC$ (Btu/hr. $ft^2\ ^oF$)

T_v is temperature of the vapor, ^oC, (^oF)

T_s is the heat sink temperature, °C, (°F)

The above heat loads must be equal, or

$$\dot{w}(h_1-h_2) = \pi D(\Delta Z)U\ (T_v - T_s) \tag{27}$$

and the required condenser length for superheat removal

$$\Delta Z = \frac{1}{\pi D}\ \frac{\dot{w}(h_1 - h_2)}{U(T_v - T_s)} \tag{28}$$

The local condensation heat transfer coefficients may be determined from a technique outlined in Reference 20. These are

$$h_z = \frac{Q/A}{t_v - t_s} \tag{29}$$

$$0.1 < F(X_{tt}) < 1.0;\quad \frac{Nu\ F_2}{Pr_\ell\ Re_\ell} = F(X_{tt}) \tag{30}$$

$$1.0 < F(X_{tt}) < 20.0;\quad \frac{Nu\ F_2}{Pr_\ell\ Re_\ell^{0.9}} = [F(X_{tt})]^{1.15} \tag{31}$$

where

$$F(X_{tt}) \equiv 0.15[X_{tt}^{-1.0} + 2.85X_{tt}^{-0.476}]$$

$$X_{tt} \equiv \left(\frac{\mu_\ell}{\mu_v}\right)^{0.1} \left(\frac{1-x}{x}\right)^{0.9} \left(\frac{\rho_v}{\rho_\ell}\right)^{0.5}$$

$$Re_\ell < 50.0; \qquad F_2 = 0.707\ Pr_\ell\ Re_\ell^{0.5}$$

$$50.0 < Re_\ell < 1125.0; \quad F_2 = 5\ Pr_\ell + 5\ \ln[1 + Pr_\ell(0.09636\ Re_\ell^{0.585} - 1)]$$

$$Re_\ell > 1125.0; \qquad F_2 = 5\ Pr_\ell + 5\ \ln\ (1 + 5\ Pr_\ell) + 2.5\ \ln(0.0031\ Re_\ell^{0.812})$$

The condensate Reynolds number is given by:

$$Re_\ell = \frac{(1-x)GD}{\mu_\ell}$$

In the above equations, μ is viscosity, G is mass flow rate per unit area, R_e is Reynolds number, Pr is Prandtl number, and Nu is the Nusselt number. A heat balance for a section is then given by

$$L(w_{L2} - w_{L1}) = h_z \Delta T \pi D \Delta Z \qquad (32)$$

where L is the latent heat of vaporization. W_{L2} is the liquid mass flow rate at the section exit, and W_{L1} is the liquid mass flow rate at the section entrance.

From $X = 1 - \frac{w_\ell}{w}$; $w_\ell = (1-X)w$

and

$$w = G\ \frac{\pi D^2}{4}$$

$$w_\ell = (1-x)G\ \frac{\pi D^2}{4}$$

Substituting the above expression into the energy balance equation yields:

$$G \frac{\pi D^2}{4} (X_1 - X_2) L = h_z \Delta T \pi D \Delta Z$$

Simplifying, $1/4\ GD\Delta XL = h_z \Delta T \Delta Z$ (33)

and

$$\frac{\Delta X}{\Delta Z} = 4 \frac{h_z}{GD} \frac{\Delta T}{L} \quad (34)$$

The length of the condenser section, ΔZ, required to change the vapor quality from X_1 to X_2 is then given by:

$$\Delta Z = \frac{GL\ D\Delta X}{4\ h_z\ \Delta T} \quad (35)$$

After the local condensation heat transfer coefficients, h_z, have been computed, the average coefficient, h_m, may be computed from the following expression:

$$h_m = \frac{1}{\ell} \int_0^{\ell} h_z\, dZ \quad (36)$$

b. Determination of Condensate Film Thickness

The condensate flow rate at distance Z may be expressed as follows:

$$w_\ell = \rho_\ell\ \pi D \int_0^{\delta} U_z dy \quad (37)$$

Assuming $y << D$ over most of the tube length produces:

$$U_z \cong -\frac{g_o}{\mu_\ell} \frac{D}{4} \frac{dP}{dZ} y \quad (38)$$

From an overall force balance on element dZ,

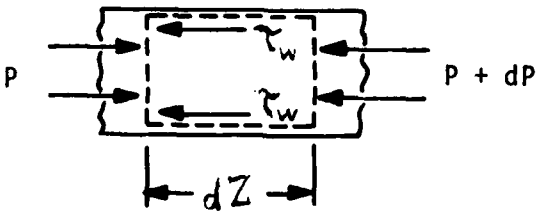

$$(P + dP - P)\ \frac{\pi}{4} D^2 = -\pi D\ dZ\ \tau_w$$

Simplifying, $\tau_w = -\frac{D}{4}\ \frac{dP}{dZ}$ (39)

where U_z is the liquid film velocity

τ_w is the shear stress on the wall

ρ_ℓ is the liquid density

μ_ℓ is the liquid viscosity

Substituting values and integrating yields:

$$w_\ell = \rho_\ell\ \pi D \int_0^\delta \frac{g_o}{\mu_\ell}\ \tau_w y dy = \frac{\pi}{2}\left(\frac{\rho_\ell g_o}{\mu_\ell}\right)\tau_w\ D\delta^2 \qquad (40)$$

where δ is the local condensate film thickness.

The above equation cannot be solved until the wall shear stress is determined. In order to determine the wall shear stress, the friction pressure drop, dP/dZ, must first be calculated. The Lockhart-Martinelli correlation (Reference 13) is often regarded as the best available method to predict the friction pressure drop, and this method is used here. The result is:

$$\left(\frac{dP}{dZ}\right)_f \frac{g_o D}{G^2/\rho_v} = -0.09\left(\frac{GD}{\mu_v}\right)^{-0.2}\left[X^{1.8} + 5.7\left(\frac{\mu_\ell}{\mu_v}\right)^{0.0523}\right.$$

$$(1-X)^{0.470}\ X^{1.33}\left(\frac{\rho_v}{\rho_\ell}\right)^{0.261} + 8.11\left(\frac{\mu_\ell}{\mu_v}\right)^{0.105}\ (1-X)^{0.94}$$

$$\left. X^{0.86}\left(\frac{\rho_v}{\rho_\ell}\right)^{0.522}\right] \qquad (41)$$

As the condensate film thickness has the largest effect on the overall heat transfer coefficients, particularly for fluids of low thermal conductivity, it is of importance to accurately predict the film thickness. It was discovered during some experimental efforts performed in-house that the above method for predicting film thickness did not provide sufficiently accurate data when the flow passages formed sharp corners. The predicted film thickness was too large. Better results were obtained when a different technique developed by W. H. Henstock and T. J. Hauratty (Reference 21) was used for predicting the condensate film thickness.

Reference 21 concludes that for $Re_\ell > 1000$ and $Re_v > 1000$ the parameter F becomes directly proportional to the Martinelli flow parameter, X_{tt}.

$$F = 0.0379X_{tt} \tag{42}$$

where

$$X_{tt} = \left(\frac{\mu_\ell}{\mu_v}\right)^{0.1} \left(\frac{\rho_v}{\rho_L}\right)^{0.5} \left(\frac{w_\ell}{w_v}\right)^{0.9}$$

The following two equations are given for determining the condensate film thickness:

(1) For horizontal flows

$$\frac{\delta}{D} = \frac{6.59F}{(1 + 850\ F)^{1/2}} \tag{43}$$

(2) For vertical flows

$$\frac{\delta}{D} = \frac{6.59\ F}{(1 + 1400F)^{1/2}} \tag{44}$$

Determination of the last item in the overall heat transfer coefficient equation will depend upon the type of condenser. The condenser can be used as a direct radiator, or it can be designed as a heat exchanger provided with a cooling fluid. Configuration and performance characteristics of these two types of condensers can be significantly different.

Before proceeding with discussions of condenser types and configurations, techniques for predicting pressure drops must be considered. There are more methods available for predicting two-phase flow pressure drop, such as: homogeneous, Thom's, Thom-Martinelli, Lockhart-Martinelli and others.

The condenser pressure drop occurs due to the friction between vapor, liquid and the tube wall, momentum change of the condensing fluid, and elevation in the gravity field. The total pressure drop may be obtained from the following expressions:

$$\frac{dP}{dZ} = \left(\frac{dP}{dZ}\right)_f + \left(\frac{dP}{dZ}\right)_m + \left(\frac{dP}{dZ}\right)_g \qquad (45)$$

where

$\left(\frac{dP}{dZ}\right)_f$ is the friction pressure drop

$\left(\frac{dP}{dZ}\right)_m$ is the momentum pressure drop

$\left(\frac{dP}{dZ}\right)_g$ is the gravity pressure drop

For a horizontal condenser, or in outer space, the gravity pressure drop can be neglected, and the expression for the total pressure drop becomes:

$$\frac{dP}{dZ} = \left(\frac{dP}{dZ}\right)_f + \left(\frac{dP}{dZ}\right)_m \tag{46}$$

Using the Lockhart-Martinelli's correlation, the friction pressure drop is expressed as already indicated.

The momentum pressure drop is:

$$\left(\frac{dP}{dZ}\right)_m \frac{Dg_o}{G^2/\rho_v} = -D\frac{dx}{dZ}\left[2x + (1-2X)\left(\frac{\rho_v}{\rho_\ell}\right)^{1/3} + (1-2x)\left(\frac{\rho_v}{\rho_\ell}\right)^{2/3} + 2(1-x)\left(\frac{\rho_v}{\rho_\ell}\right)\right] \tag{47}$$

where x is quality of the vapor and G is mass velocity of the total flow.

Dividing the quality range into several steps, the local values are to be calculated for the average quality of those steps. In calculating the momentum pressure drop term, an initial trial value of dx/dZ must be assumed. The initial value, however, should agree with the value obtained from the following expression:

$$\frac{\Delta x}{\Delta Z} = 4\frac{h_z \Delta T}{L\ DG} \tag{34}$$

If these values do not agree, the computation should be repeated.

Under actual conditions the momentum pressure gradient is small, and if it cannot be completely neglected, then a second trial usually provides a good agreement. The equations and methods described above were incorporated into a small computer program to predict the needed length and pressure drop through a straight tube condenser.

2. CONDENSER STABILITY CONSIDERATIONS

Unstable flow could result in severe oscillations, local choking, or other disturbances which could upset condenser performance. Two-phase flow in any force field is subjected to a large variety of different flow patterns. Cooling and power systems which utilize two-phase fluids often encounter such stability problems. For both boiling and condensing processes, a knowledge of the flow stability and fluid pressure drop is essential. The introduction of oscillations of certain amplitudes and frequencies might change wavy flow into slug flow, and this slug flow might cause non-steady pump and system operation.

Results of some experiments have led to the selection of annular or stable wavy annular flow as the most desirable flow regime for condensation of a wetting fluid. Bubbly and plug flow imply a very low vapor flow rate and inefficient use of the tube volume. Slug flow, in accordance with the experimental work, is the major threat to stability of a closed system. Slug flow was found to be the result of the distabilizing effects of high inlet Reynolds number, large flow area and low body forces on annular or wavy annular flow. Disturbance waves in the condensate film in the annular flow regime would grow under the proper combination of vapor shear and Bernoulli type forces until adhesive forces predominate resulting in liquid slug formation. Slug flow could be completely eliminated in a one-g field by merely increasing the vapor flow velocity.

Thin turbulator strips can also be placed in condenser to suppress unstable conditions. These strips impart swirl to the flowing fluid and seem to eliminate oscillations.

Use of a curved flow passage can also provide large body forces on the condensate layer and result in a stabilizing effect on wave formation and growth. Tapering the tubes is another method of maintaining vapor shear on the condensate film to suppress liquid wave growth and improve stability.

Miles (Reference 22) has determined that, for large liquid Reynolds numbers, i.e., $Re_L \to \infty$, a sufficient condition for stability is that the Weber numbers (N_W) be less than 3. As a lower bound, he found that there exists a critical liquid Reynolds number below which the flow will always be stable. His calculations indicate that the value of this Reynolds number is approximately 200. Therefore:

$$N_W = \frac{\rho_\ell U_i^2 \delta}{g_c \sigma} \leq 3 \text{ for stability} \qquad (48)$$

or

$$Re_\ell = \frac{\rho_\ell U_i \delta}{\mu_\ell} \leq 200 \text{ for stability}$$

It may be seen from the above equations that the criteria for hydrodynamic stability during annular flow may be determined by calculating liquid free surface velocity and film thickness. Since these parameters change over the entire length of the condenser passage, the Weber and liquid Reynolds number must be evaluated over the entire length.

Several investigators, however, have suggested that tapered tubes are necessary to produce stable flow in zero-g condensation. They reason that reducing tube diameter in the direction of the flow increases the vapor velocity, thus helping prevent bridging of liquid across the tube. It has also been suggested that the use of orifices in each tube at the liquid manifold would produce a more stable flow.

Reference 23 presents a study under which a condensing space radiator for use in a spacecraft vapor compression refrigeration system was developed and tested in both gravity and zero-gravity environments. The study investigated two-phase flow and pressure drop for small diameter tubes where capillary action is significant. This and other studies have indicated that stable transition to slug flow occurs in small (capillary) tubes, particularly when under zero-gravity condition.

As a conseqence of liquid velocity decline during condensation, interfacial or Taylor instability can occur when gravity causes the interface to collapse. This type of instability is a function of the tube diameter and the local acceleration field. Denington (Reference 24) has defined the maximum stable tube diameter as:

$$D \leq 1.835 \left[\frac{\sigma}{(\rho_\ell - \rho_v)n}\right]^{1/2} \tag{49}$$

where

σ is the surface tension

ρ_ℓ and ρ_v are the liquid and vapor densities, respectively, and

n is the ratio of local acceleration of gravity to g_o.

The following conditions imposed on a two-phase flow can be helpful in achieving stable system operation:

(1) Annular flow is the most desirable for stable operation,

(2) Tapering the flow passages,

(3) Passage curvature, and

(4) Turbulator strips.

3. FLOW PATTERN MAPS

Results of different correlations show that different methods can give vastly divergent results, differing by a factor of 10 or more for a given set of conditions. Efforts have been made by some investigators to select flow map coordinates based on force balance criteria, while others have used stress ratio defined as the ratio of axial shear force to gravitational body force. Palen, et al. (Reference 25) found that shear controlled regimes (annular, mist annular) and gravity controlled regimes (wavy, stratified, slug) are quite well separated by dimensionless gas velocity, $j_g^* = 1$. Generally, the transition values were within $j_g^* = 0.5$ and $j_g = 1.5$. The mist and mist-annular data were found to fall above $j_g^* = 5$.

A flow regime map has been developed with dimensionless gas velocity j_g^* as ordinate and Martinelli parameter X as abscissa. While the map was found to give good agreement with moderate and large tube diameters, agreement with experimental data for wavy and slug flows with a small tube diameter was poor.

Reference 26 presents a simplified flow regime map for two-phase flow patterns during condensation inside horizontal tubes. The data are based on 664 flow pattern observations resulting from 349 runs used in the development of the flow regime map. To correlate this data, the force balance approach resulted in a dimensionless group that was termed by Wallis as dimensionless gas velocity, j_g^*, defined as

$$j_g^* = \frac{XG}{[gD\rho_v(\rho_L - \rho_v)]^{1/2}}$$

The void friction, α, which significantly characterizes the two-phase flow pattern, was selected as the other parameter. α has been calculated from Smith's equation given as

$$\alpha = \left\{ 1 + \left(\frac{\rho_v}{\rho_\ell}\right)\left(\frac{1-x}{x}\right) \left[0.4 + 0.6\sqrt{\frac{\frac{\rho_L}{\rho_v} + 0.4\left(\frac{1-x}{x}\right)}{1 + 0.4\left(\frac{1-x}{x}\right)}} \right] \right\}^{-1} \quad (50)$$

The above equation has been developed using a large number of experimental data of several investigators. The equation should be valid for all flow condition irrespective of flow patterns, mass velocity or pressure. Figure 24 shows the simplified map of the flow patterns.

4. CONDENSING RADIATORS

Design of a radiator requires information about the expected temperatures that the spacecraft and/or radiator will experience during its mission and particular orbit. Accurate prediction of these temperatures will require knowledge of the natural environment which

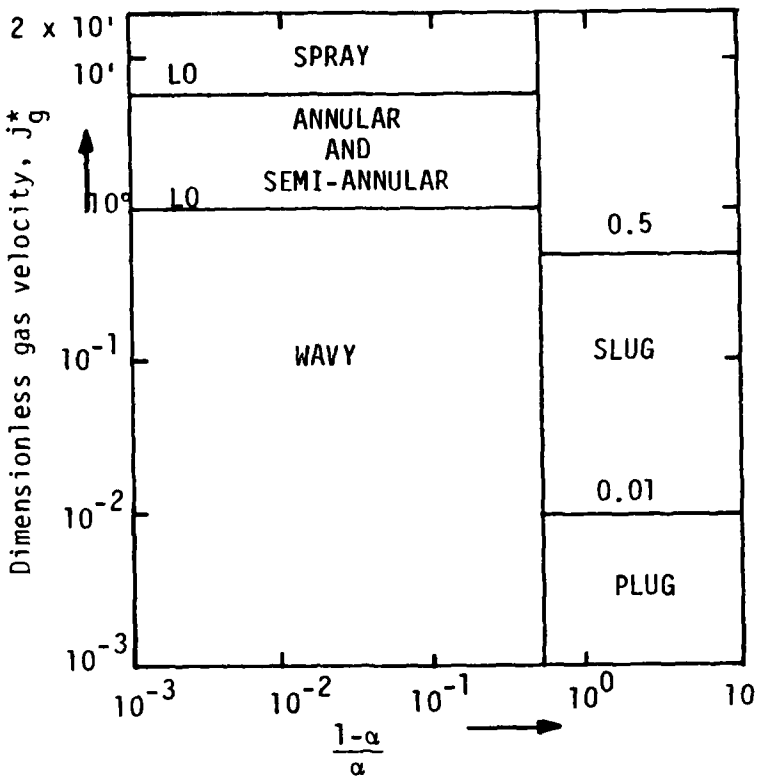

Figure 24. Proposed Simplified Criteria for Flow Patterns During Condensation Inside Horizontal Tubes (Reference 26)

includes high vacuum, solar radiation and planetary albedo and emission. Except for highly simplified models, high-speed computer techniques are generally required for detailed thermal analysis of radiators on spacecraft.

Only a general analysis technique will be presented here for a flat tube-fin type radiator. As condensation takes place within the tubes, the temperatue of the tubes, and thus also the fin root, can be assumed as constant. The heat of condensation removed from the vapor must be dissipated to outer space by the radiating fins.

The heat dissipation rate from the fins may be determined by deriving an energy balance for a fin element as shown in Figure 25.

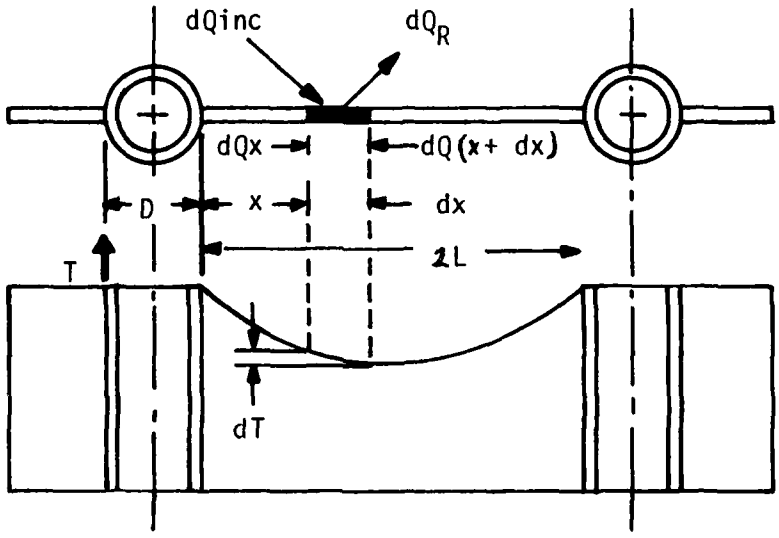

Figure 25. Radiator Fin Element

Neglecting irradiation between the fin element and tubes, the following expression can be written for an instantaneous heat balance:

$$\text{Heat in} = \text{Heat out}$$

or

$$dQx + dQinc = dQ_R + dQ(x+ dx) \tag{51}$$

where

$$dQx = -kA\frac{dT}{dx}$$

dQ_{inc} consists of direct radiation streaming from the sun, radiation from the earth, and earth reflected solar radiation, or

$$dQ_{inc} = k_1 E_s \alpha_s dA_s + k_2 r_e E_s F \alpha_s dA_e + E_e F \epsilon dA_e \tag{52}$$

and

$$Q_{inc} = k_1 E_s \alpha_s A_s + k_2 r_e E_s F \alpha_s A_e + E_e F \epsilon A_e \tag{53}$$

where:

k_1 = fraction of orbit time in sunlight

E_s = solar constant

α_s = solar absorptance

A_s = projected area of radiator normal to sun

k_2 = fraction of orbit time radiator is exposed to earth reflected sunlight

r_e = earth albedo

F = view factor for earth to radiator radiation

ε = infrared emittance

A_e = projected area of radiator normal to earth

E_e = earth emissive power

F_f = view factor of fin

$$dQ_r = \varepsilon\sigma \, dA_x \, F_f \, (T_x^4 - T_s^4)$$

where $dA_x = Bdx$

and for a unit width of the element or when $B = 1$,

$$dA_x = dx$$

Substituting this value yields

$$dQ_R = \varepsilon\sigma \, F_f \, (T_x^4 - T_s^4) \, dx$$

When both sides of the fin are radiating,

$$dQ_R = 2\varepsilon\sigma \, F_f \, (T_x^4 - T_s^4) \, dx$$

Returning to the balance equation, one obtains

$$dQ_x + dx = -kA \left(\frac{dT}{dx} + \frac{d^2T}{dx^2} \, dx \right)$$

Substituting values into the heat balance equation yields

$$-kA \frac{dT}{dx} + k_1 E_s \alpha_s dA_s + k_2 r_e F E_s \alpha_s dA_e + E_e F \epsilon dA_e$$

$$= 2\epsilon\sigma F_f (T_x^4 - T_s^4) dx - kA \left(\frac{dT}{dx} + \frac{d^2T}{dx^2} dx\right)$$

or

$$-kA \frac{dT}{dx} + dQ_{inc} = 2\epsilon\sigma F_f (T_x^4 - T_s^4) dx - kA \left(\frac{dT}{dx} + \frac{d^2T}{dx^2} dx\right)$$

Simplying and rearranging, this equation produces

$$kA \frac{d^2T}{dx^2} dx = 2\epsilon\sigma F_f (T_x^4 - T_s^4) dx - d Q_{inc} \quad (54)$$

Again basing the heat balance on unit width of the radiator, $dA_x = (1)dx = dx$, the expression for dQ_{inc} can be modified as follows:

$$dQ_{inc} = k_1 E_s \alpha dx + k_2 r_e F E_s \alpha dx + E_e F \epsilon dx =$$

$$(k_1 E_s \alpha + k_2 r_e F E_s \alpha_s + E_e F \epsilon) dx =$$

$$(C_1 + C_2 + C_3) dx = C dx$$

Substituting the above value into the heat balance equation yields

$$kA \frac{d^2T}{dx^2} dx = 2\epsilon\sigma F_f (T_x^4 - T_s^4) dx - C d_x$$

or

$$kA \frac{d^2T}{dx^2} = 2\epsilon\sigma F_f (T_x^4 - T_s^4) - C \quad (55)$$

Expressing the heat flow area per unit width of the radiator as

$$A = (1) \delta = \delta,$$

$$\frac{d^2T}{dx^2} = \frac{1}{k\delta} [2\epsilon\sigma F_f (T_x^4 - T_s^4) - C] \quad (56)$$

The above equation is the differential equation for the temperature distribution along the fin normal to fluid flow. The equation can be solved by computer techniques applying the following boundary conditions:

(1) At $x = 0$, $T_x = T_b$

(2) At $x = L$, $\frac{dT}{dx} \approx 0$

When the temperature distribution of the fin is known, the radiant heat rejection rate may also be determined if the space heat sink temperature is known. The net radiant heat rejected from a surface area is the difference between the emitted and incident radiation, or

$$dQ_{net} = dQ_r - dQ_{inc}$$

Substituting values and integrating yields

$$Q_{net} = 2\varepsilon\sigma F_f \int_0^L (T_x^4 - T_s^4)dx - C_0 \int_0^L dx \tag{57}$$

Actually, heat rejected from the radiator can be considered as consisting of two parts: (1) heat rejected from fins, and (2) heat rejected from the base surfaces (tubes), or

$$Q = Q_f + Q_t \tag{58}$$

Neglecting the short superheat and subcooling sections of the condenser, the tubes may be assumed as constant temperature sections, and the heat dissipation rate from the tubes can be expressed as follows:

$$Q_t = A_t \varepsilon\sigma F_t (T_b^4 - T_s^4) - Q_{inc,t} \tag{59}$$

where

$$A_t = (\pi D - 2\delta)(1) = \pi D - 2\delta$$

Total heat dissipated from a radiator section will be:

$$Q_{net,tot} = 2\varepsilon\sigma F_f \int_0^L (T_x^4 - T_s^4)dx - C \int_0^L dx + \frac{1}{2} A_e \varepsilon\sigma F_t (T_b^4 - T_s^4) - \frac{1}{2} Q_{inc,t} \quad (60)$$

It should be noted that in computing incident radiation to the tube, the tube's projected area must be used.

Considering now heat removal from the condensing vapor, heat dissipated from the radiator section must equal the enthalpy change of the fluid. Referring to Figure 26, the following expression can be developed for a condenser section:

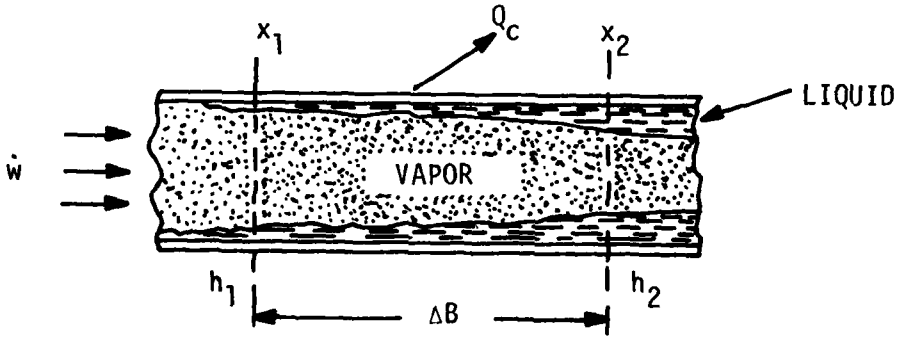

Figure 26. Condenser Element

$$Q_c = \dot{w} (h_1 - h_2)$$

where

$$h_1 = X_1 h_g + (1 - X_1)h_L$$

$$h_2 = x_2 h_g (1 - X_2)h_L$$

Substituting, simplifying and rearranging provide:

$$Q_c = \dot{w} (x_1 - x_2) (h_g - h_L) \quad (61)$$

$$Q_c = Q_{net,tot}$$

From the computed heat dissipation rate of the condenser section, quality change of the vapor can be determined from the following expression:

$$(x_1 - x_2) = \Delta x = \frac{Q_{net,tot}}{\dot{w}\,(h_g - h_L)} \qquad (62)$$

Flow stability of the directly condensing radiators could be improved by tapering the tubes or inserting turbulator strips into the tubes as shown in Figure 27.

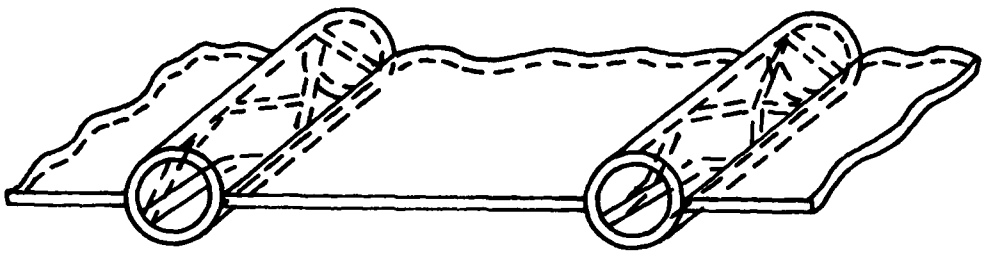

Figure 27. Radiator Section with Turbulator Strips

Although such strips or twisted tapes will increase pressure drop of the condenser, they will improve flow stability and increase the heat transfer surface area. Another advantage, although not significant, is some improvement in the condensation heat transfer coefficient resulting from reduction of the condensate film thickness build-up. It is anticipated that such condensers will not require introduction of large artificial body forces, and the penalties, as far as pressure drops is concerned, will not be large. Alternatives to the direct condensing radiator, such as a condensing heat exchanger at the base of a heat pipe radiator, must also be considered.

5. FLOW DISTRIBUTIONS IN THE MANIFOLDS

Proper flow distribution in any type of heat transfer device (heat exchanger) where flow passages are in parallel is of importance. In numerous heat exchanger configurations, particularly in condensing radiators, the flow passages are arranged in parallel. When heat transfer computations are performed, it is usually assumed that an ideal velocity and flow distribution takes place within the flow passages.

Under actual conditions, however, large deviations from the ideal flow distribution can occur.

Two main factors , inertia and friction, determine the distribution of flow in and out of the manifolds. When the inlet manifold has a constant cross section, the velocity reduction in the direction of flow leads to a conversion of velocity pressure into static pressure. The opposite occurs in the discharge manifold. On the other hand, friction causes loss of pressure along the manifold, or in any flow passage. The relative magnitude of the pressure regained because of the reduced velocity and the pressure loss because of friction determine whether the pressure rises or falls from the inlet end to the closed end of the manifold. If the cross section of the manifold can be changed, it is possible to size the area along the length in a manner that the two opposing factors balance each other, resulting in a uniform discharge along the length.

Figure 28 shows a radiator configuration with manifolds of constant cross-sectioned area.

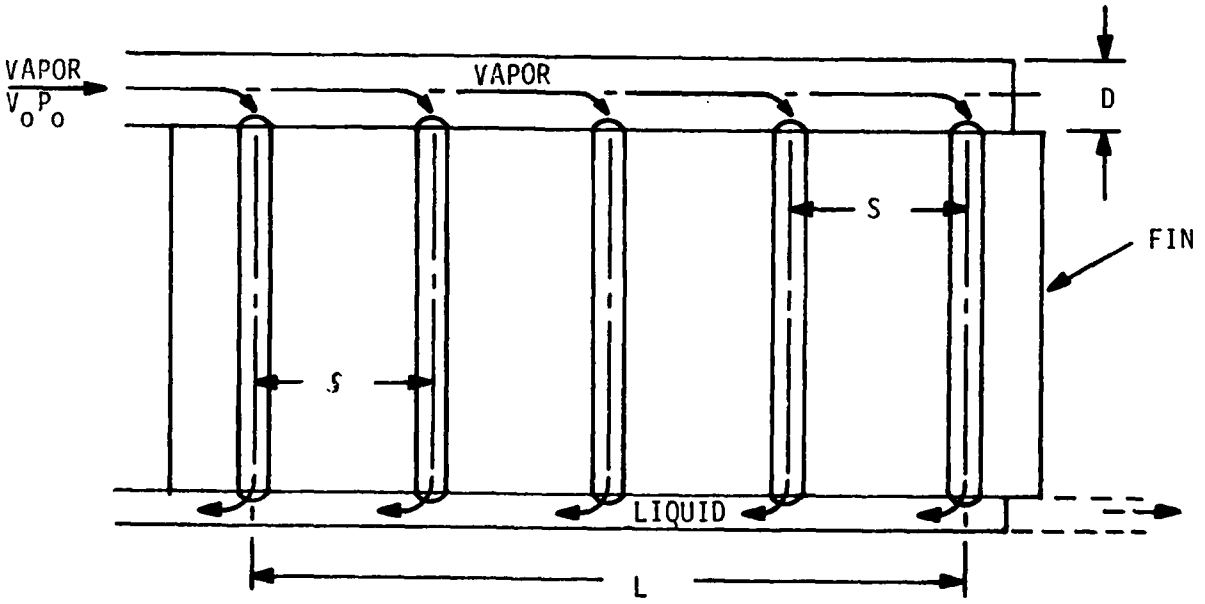

Figure 28. Manifold Schematic

Reference 27 gives the following expression for discharge velocity variation at distances from the dead end of the manifold shown in Figure 28.

$$V_1 = \frac{V_o}{\sin(kR)} \cos\left(kR \frac{S}{L}\right) \qquad (63)$$

where V_o = inlet flow velocity

L = length of manifold

k = coefficient of discharge of the holes

R = $\frac{\text{sum of areas of all discharge openings}}{\text{cross sectional area of manifold}}$

In accordance with Reference 27, for a ratio L/D = 70, the friction practically cancels the deceleration regain, and the distribution of discharge along the length is practically constant. There is, however, another item of concern, and that is the area ratio. The same reference points out that for an area ratio of R = 2, the variation is much greater; and, regardless of the length/diameter ratio, it is not possible to obtain a satisfactory uniformity of discharge. When the area ratio is increased still further, a condition can be reached where the discharge rate at the inlet end reduces to zero, or even reverses. Friction, however, has an equalizing effect; the greater the L/D, the greater the area ratio can be without causing the flow to reverse.

When inlet and outlet manifolds are at the same side (as shown on Figure 28), the pressure variation in one manifold tends to counteract that in the other manifold, thus providing more uniform flow distribution. An exception to this case is manifolds with very large L/D ratios where the friction loss far outweighs deceleration regain. In such a case, the inlet and outlet ends should be at opposite sides (shown with broken lines).

Another method for ensuring uniform flow distribution throughout a tube bank is to maintain constant flow velocity by reducing the cross-sectional area of the manifold. The contour can usually be so changed that friction loss counterbalances deceleration regain. Thus, the pressure can be caused to remain constant along the flow path. If friction could be neglected, then the only requirement for uniform discharge would be to maintain the longitudinal velocity constant. This condition could be achieved by decreasing the cross-sectional area linearly from the maximum at the inlet to zero at the dead end. Reference 27 presents the following expression for a manifold of circular cross-section:

$$D = (D_o + fgL)\sqrt{\frac{S}{L}} - fgS \qquad (64)$$

where: D = diameter at a distance S from the dead end

D_o = diameter at inlet end

L = actual length of manifold

f = friction coefficient ~ 0.00052

g = acceleration of gravity

Reference 28 presents a parabolic manifold geometry, including a computer program for designing such manifolds. Figure 29 shows an outline of the parabolic manifold.

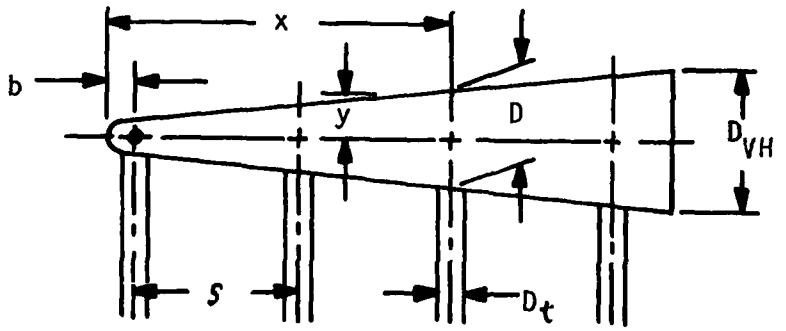

Figure 29. Parabolic Manifold

The vapor manifold is made of a symmetrical section generated by a rotating parabola given by the equation

$$y^2 = 4\ bx$$

where the constant b describes the distance from the vertex of the parabola to its focal point as shown in the figure.

6. CONDENSATION PROCESS SUMMARY

Predictions can differ from actual test data by as much as $\pm$ 25 percent, depending upon the conditions and condenser configurations. For stability and efficiency reasons, the tapered tube condenser seems to be the choice for space applications. Reducing the diameter in the direction of flow helps keep the vapor velocity constant and the film thickness small. A small film thickness provides a higher overall heat transfer coefficient, thereby increasing the efficiency of the condenser and reducing the probability of slug or plug flow instabilities.

Further experimental verification and testing in one-g and zero-g environments is necessary along with a better theoretical understanding of two-phase fluid behavior. This will yield the more accurate methods needed to predict flow stability, heat transfer rate, length, and pressure drops through the condenser. This will also show where further refinements are necessary.

SECTION IV

TWO-PHASE FLOW PATTERNS

1. FLOW PATTERN ANALYSIS REVIEW

In order to design an advanced two-phase cooling loop for spacecraft applications, we need to be able to analyze the flow within the system and predict the heat transfer coefficients and pressure drops for both ground testing and "zero-g" operation. Unfortunately, analysis and design involving two-phase flows have no comprehensive mathematical models to relate pressure drop with other parameters (Reference 29). Many investigators have developed empirical correlations for heat transfer coefficients and pressure drop, but these correlations are good only for their respective flow regimes. The key, then, to predicting heat transfer and pressure drop is to first be able to predict the flow regime present.

A flow regime is a characteristic spatial distribution of the liquid and gas flows. When different forces dominate the flow, different flow regimes will be encountered. The various flow regimes or flow patterns will exert different effects on the hydrodynamic conditions near the wall and cause different frictional pressure drops and different modes of heat transfer (Reference 30).

The flow regimes of interest are: stratified, slug, churn, bubbly disperse, bubbly annular, annular, and dispersed mist (Figure 30). Churn flow is unstable slug flow and is an entry length phenomenon. However, for many engineering applications the entry length will comprise the entire channel length of interest. Another point of interest here is that there is a distinction made between bubbly annular and annular flow. Bubbly annular flow is annular flow with boiling taking place. Annular flow is flow with evaporation or condensation at the interface, and the only mode of heat transfer to the wall is conduction.

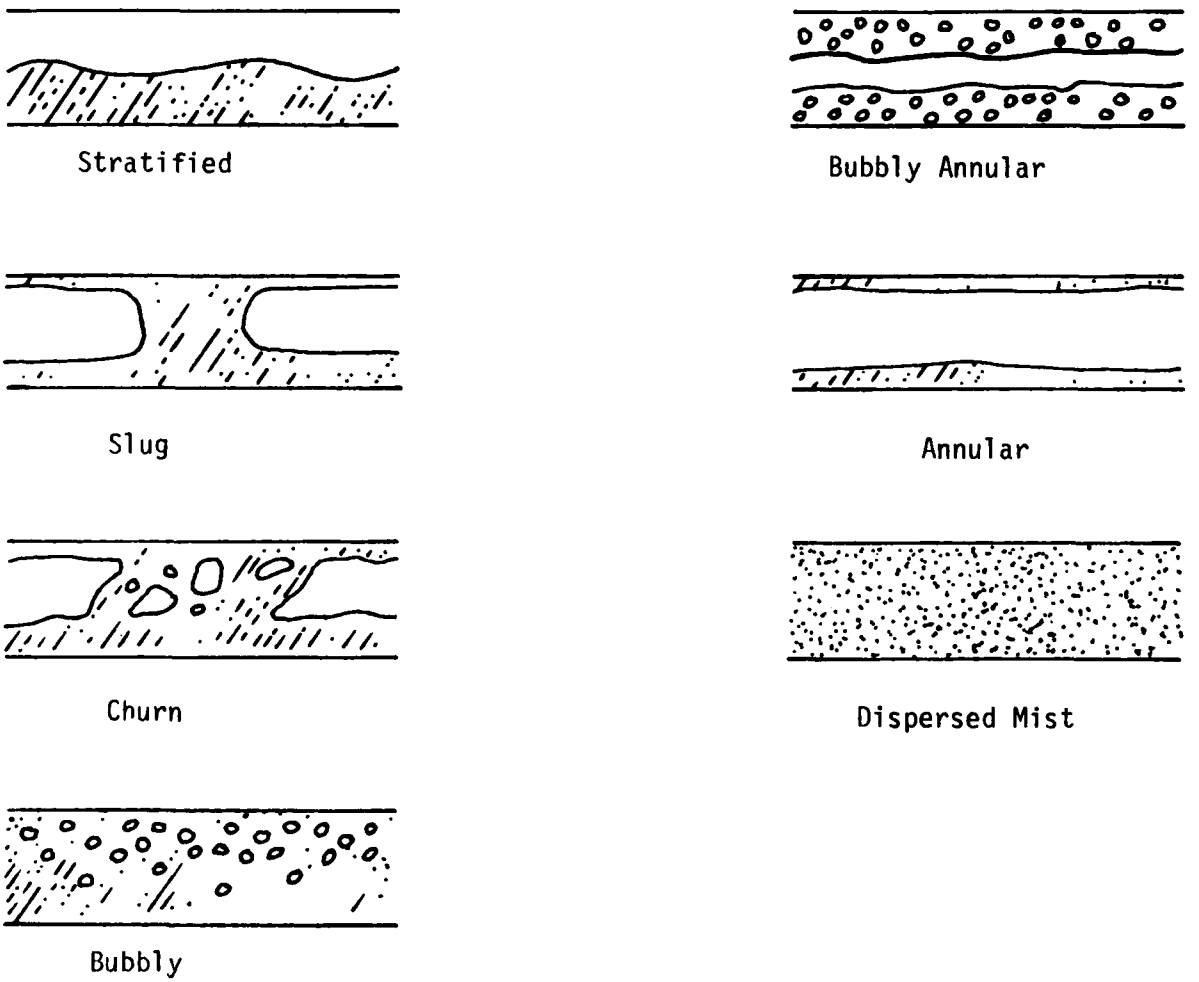

Figure 30. Typical Flow Patterns

The forces that act on the flow to cause the various flow regimes are: gravity, surface tension, inertia, frictional drag, and the Bernoulli effect. Gravity tends to stabilize the flow and create a stratified flow pattern. Surface tension tends to wick the fluid around the circumference of the pipe creating annular flows and it tends to create strong interfacial forces which lead to slug flow. The inertia force manifests itself in turbulent fluctuations which create disperse flows, while the frictional drag causes pressure differentials that tend to create stratified and annular flows. And finally, the Bernoulli effect causes waves to be generated in annular and stratified flow regimes, and it causes bubbles in bubbly flows to migrate toward the center creating annular flows.

Many investigators have attempted to quantitatively predict the flow regime boundaries for specified conditions. However, most of these methods are only good for the circumstances in which they were developed, and great care must be taken in using them for other conditions. Some of the especially pertinent references are reviewed in the following paragraphs.

Probably the most well known and one of the oldest attempts at predicting flow regime transitions was done by Ovid Baker (Reference 31). The work is based on data from adiabatic flows of air and water in horizontal pipes. The equations derived are entirely empirical and use the parameters G_g/λ and $\lambda 4G_\ell/G_g \cdot G_g$ and G_ℓ are the vapor and liquid mass flow rates based on total cross-sectional area of the pipe. The other values are defined as:

$$\lambda = \left[(\rho_g/0.075)\ (\rho_\ell/62.3)\right]^{1/2}$$

and

$$\psi = \left[\left((73/\sigma)\mu_\ell\right)\ (62.3/\rho_\ell)^2\right]^{1/3}$$

A typical Baker Plot is shown in Figure 31.

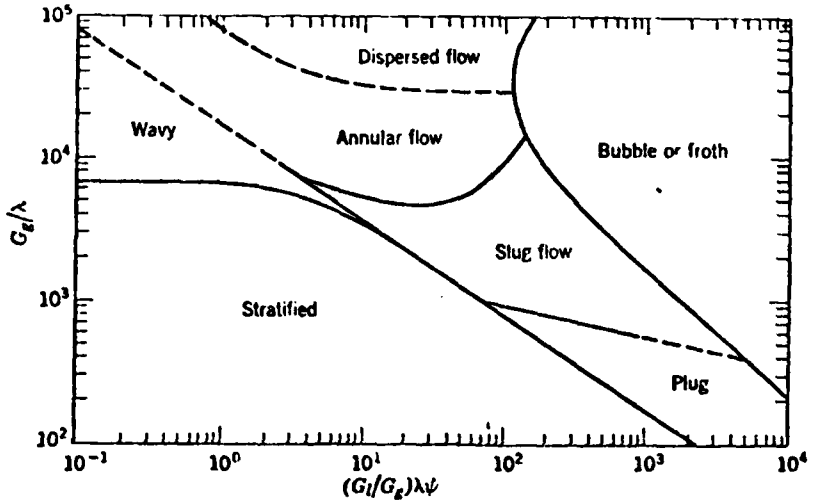

Figure 31. Flow Regimes as Designated by Baker

M. Suo and P. Griffith (Reference 32) examined the flow of long bubbles and liquid slugs in capillary tubes. The analysis considers pressure and viscosity effects so that velocity ratios between the vapor and liquid can be estimated. This leads to a predicted transition from slug to annular flow as the vapor to liquid volume ratio is increased. Another transition from slug to bubbly-slug flow is predicted when the velocity increases so that the Reynolds number, Weber number ($W_b = \frac{\rho v^2 D}{\sigma}$) product exceeds 2.8×10^5. The analysis is for Bond numbers ($B_o = \rho g D^2/\sigma$) less than 0.22 and is shown to provide agreement in form with experimental data although the predicted boundary location is only approximate. Liquid boundary layer thickness for these flow conditions may also be estimated from the analysis for zero-g.

Quandt (Reference 33) presented an analysis to predict basic flow patterns by considering the dominant force acting on the fluid under particular conditions. With simplifying assumptions, these forces are: axial pressure gradient, gravitational attraction, and interfacial surface tension. The mixture Froude ($F_r = v^2/gD$) and Weber numbers cam be used to indicate which force is dominant. Surface tension is expected to be important only in tubes with one cm. or smaller diameter. Dispersed flows at high mass velocities are pressure gradient dominated, while low velocity flows (slug, stratified and wave) tend to be highly

influenced by body forces such as gravity. These force considerations also lead to a prediction of slug flow for a Froude number less than 2/f where f is the friction factor of a single phase and the Froude number is based on a homogeneous mixture velocity and density. Froude numbers of 60 to 80 are said to be typical for the transition from slug to annular flow. Other approximate criteria are given for bubble and rivulet flow at low and high quality respectively.

In 1975, an interesting paper was presented by D. B. Heppner, C. D. King, and J. W. Littles (Reference 34). The Quandt approach was modified with other considerations to predict transitions among three basic types of flow: (1) segregated (stratified, wave, annular), (2) intermittent (plug, slug), and (3) distributed (one phase continuous). The theory indicates a shift toward distributed flows at low "g" levels with the intermittent and segregated flows restricted to narrower ranges of quality and velocity. Some shifts in that direction were experimentally observed during aircraft flights, but the shifts were not so great as analytically predicted. Another set of flight tests produced shifts close to the predicted magnitude. The tests were conducted with air and water mixtures. One important result was the demonstration of larger pressure drops at zero-g than at one-g. This was attributed to flow regime transitions toward more turbulent flow. While giving some indications of expected flow pattern shifts, the methods presented in this paper are not highly useful in calculating flow regime boundaries, especially for low quality (<.01) flows.

Another approach to predicting flow regimes is described in a 1976 paper by Y. Taitel and A. E. Dukler (Reference 35). Since the exact sequence in which a given flow pattern develops may be analytically unimportant after the conditions for the pattern are established, the authors started with an assumption of stratified flow and examined transitions to slug/plug and annular flow. By considering the stability of waves on the liquid surface in stratified flow, transitions can be predicted. Wave growth is aided by low vapor pressure over the crest caused by the Bernoulli effect. Growth is retarded by the weight and viscosity of the liquid. Considering only the weight effects, the waves will grow when

$$U_g \geq \sqrt{\frac{g(\rho_\ell - \rho_g) h_g}{\rho_g}}$$

where U_g is the vapor velocity, ρ refers to density, and h_g is the distance between the liquid surface and top of the channel.

Modifications to this simple criteria are given to account for circular ducts and friction effects. While the equations only indicate that transitions from stratified flow would always occur at zero-g, they can be used to show flow pattern boundaries at low "g" levels. This is shown in Figure 32 where space experiments (Reference 36) are planned at two different g levels to show the different flow patterns. However, Figure 32 does not take into consideration the laminar flow of the liquid at low velocities or the effect of surface tension. Experiments by other investigators have verified that transitions to slug/plug flow will occur if the channel is more than half filled with liquid. This is pictured as a wave growth in which the crest reaches the top of the channel. Lower liquid levels may transition to annular flow if the vapor velocity is sufficiently high. When the liquid level and velocity are both sufficiently high, the gas tends to mix with the liquid, and transitions to dispersed bubble flow will occur as the turbulence increases. The existence of this dispersed flow at lower mass velocities as the "g" level decreases would be consistent with discussions in earlier technical papers.

In the late 1970s, Weisman, et al. (References 37 and 38) conducted numerous experiments to determine the effects of different properties on flow pattern transitions. Using an air/aqueous loop, they systematically varied test section diameter, liquid viscosity, liquid surface tension, liquid density, and vapor density. These experiments were carried out in horizontal, inclined, and vertical pipes.

Unfortunately, for our purposes, most of these analyses are incomplete. The reason is that most of the work was done in support of the petroleum industry and nuclear reactors. The problem with that is that the investigators were concerned with large diameter tubes under unvarying gravitational conditions. The use of large diameter tubes and

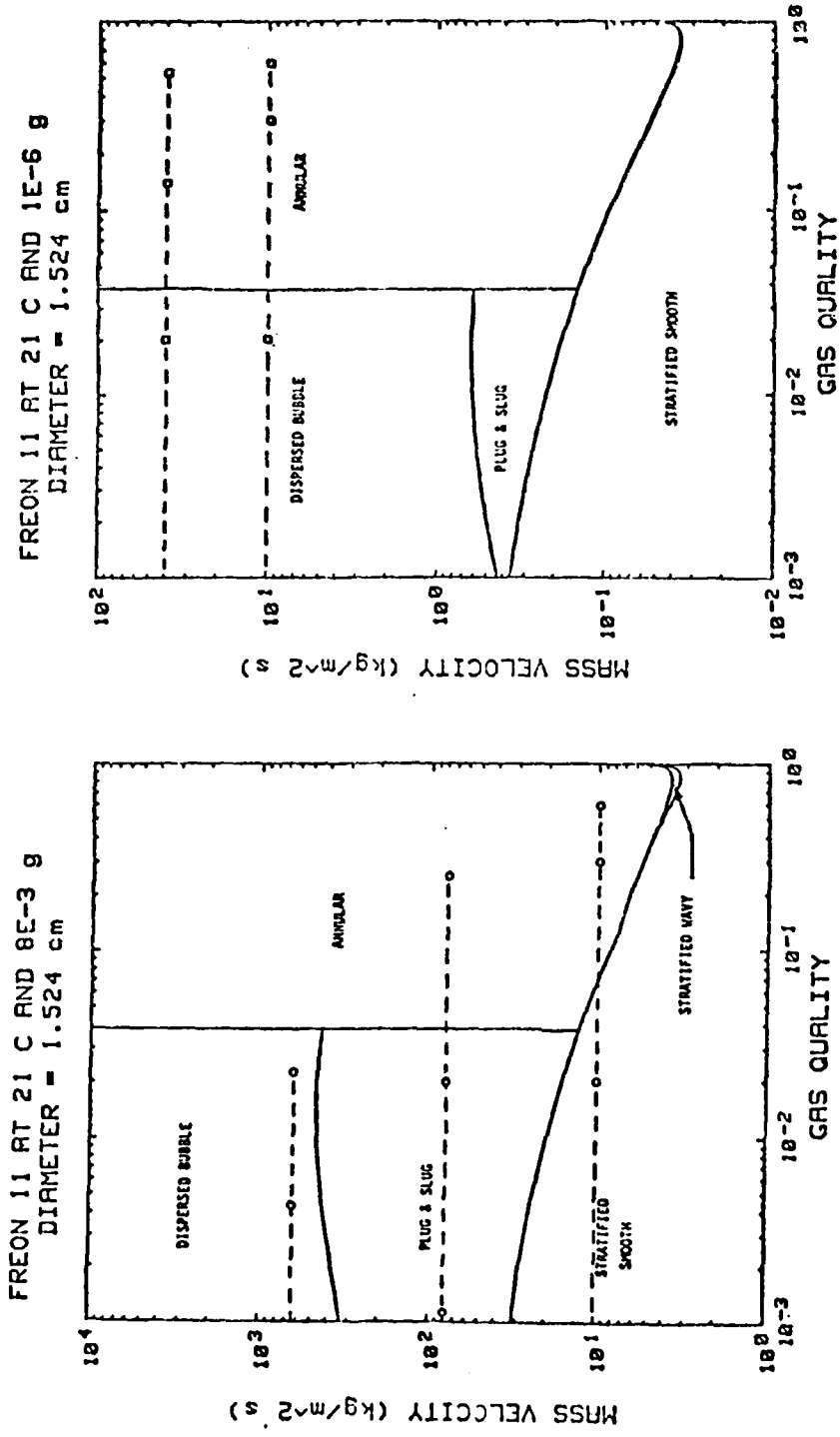

Figure 32. Flow Boiling Regime Prediction

a 1-g field allowed these investigators to almost completely ignore the effects of surface tension. For small diameter tubes and/or low gravitational acceleration, surface tension plays a major role in determining the flow regime present. Only a very few investigators consider surface tension and small diameter efffects, and their work is incomplete for successfully "mapping" flow regimes under low gravitational accelerations.

2. SUGGESTED TRANSITION CRITERIA

In spite of deficiencies mentioned previously, it appears that the best transition criteria available at this time are those developed by Weisman et al. (References 37 and 38) Although there are some discrepancies at extremely small gravitational accelerations and for extremely small tubes, their work seems to be the most complete and accurate to date. The flow regimes used are: intermittent, stratified, annular, and disperse. Intermittent includes slug and churn flow, while disperse includes both forth and mist flows. The following are the criteria governing the transition regions:

Intermittent to Stratified (horizontal)

$$G = \frac{1}{x} \left(\frac{x}{1-x}\right)^{1.1} \sqrt{g} \left\{0.25\, \rho_g \sqrt{D} \left(\frac{\rho_\ell}{\rho_g}\right)^{1.1}\right\}$$

with

$$A = 0.25\, \rho_g \left(\frac{\rho_\ell}{\rho_g}\right)^{1.1}$$

then:

$$G = A \frac{1}{x} \left(\frac{x}{1-x}\right)^{1.1} \sqrt{g} \qquad (65)$$

Intermittent/Stratified to Annular (vertical or horizontal)

$$G = \frac{1}{x} \left(\frac{x}{1-x}\right)^{0.2232} g^{0.4107} \left\{3.1461 \left(\frac{\rho_\ell}{\rho_g}\right)^{0.2232} \rho_g^{0.8214} [(\rho_\ell - \rho_g)\sigma]^{0.0893} D^{0.3214}\right\}$$

with

$$B = \left\{3.1461 \left(\frac{\rho_\ell}{\rho_g}\right)^{0.2232} \rho_g^{0.8214} [(\rho_\ell - \rho_g)\sigma]^{0.0893} D^{0.3214}\right\}$$

then

$$G = B \frac{1}{x} \left(\frac{x}{1-x}\right)^{0.2232} g^{0.4107} \qquad (66)$$

Intermittent/Annular to Disperse (vertical or horizontal)

$$G = \left(\frac{1}{1-x}\right) g^{1/4} \left\{13.72\ \rho_\ell^{1/2}(\rho_\ell-\rho_g)^{1/4}\ \sigma^{1/4}\ \left(\frac{1}{f'}\right)^{1/2}\right\}$$

with

$$C = \left\{13.72\ \rho_\ell^{1/2}\ (\rho_\ell - \rho_g)^{1/4}\ \sigma^{1/4}\ \left(\frac{1}{f'}\right)^{1/2}\right\}$$

then

$$G = \left(\frac{1}{1-x}\right)_g^{1/4} C \qquad (67)$$

Stratified Smooth to Stratified Wavy (horizontal)

$$G = \frac{1}{x}\left(\frac{x}{1-x}\right)^{0.3556} g^{0.4444} \left\{101.6\mu_g\ D^{-0.1111}\ \left(\frac{\rho_\ell}{\rho_g}\right)^{0.3556}\ (\rho_\ell-\rho_g)^{0.4444}\ \sigma^{-0.4444}\right\}$$

with

$$E = 101.6\ \mu_g\ D^{-0.1111}\ \left(\frac{\rho_\ell}{\rho_g}\right)^{0.3556}\ (\rho_\ell-\rho_g)^{0.4444}\ \sigma^{-0.4444}\Big\}$$

then

$$G = E\ \frac{1}{x}\ \left(\frac{x}{1-x}\right)^{0.3556} g^{0.4444} \qquad (68)$$

Intermittent to Bubble (vertical and upwardly inclined)

$$G = \left(\frac{1}{x}\right)^{4.5455} \left(\frac{x}{\rho_g} + \frac{(1-x)}{\rho_g}\right)^{3.5455} g^{1/2} \left\{(0.0265)D^{1/2}\ \rho_g^{4.5455}\ (1-\ .65\cos\theta)^{4.5455}\right\}$$

with

$$F = 0.0265\ D^{1/2}\ \rho_g^{4.5455}\ (1 - 0.65\ \cos\theta)^{4.5455}$$

then

$$G = F\ \left(\frac{1}{x}\right)^{4.5455} \left(\frac{x}{\rho_g} + \frac{(1-x)}{\rho_\ell}\right)^{3.5455} g^{1/2} \qquad (69)$$

Stratified flow does not appear for $\sin\theta > D/L$

As mentioned previously, these transition criteria are not quite accurate at very low accelerations or for very small diameter tubes. In particular, there are no specific limits of small tube diameter or low gravitational effect which would allow the liquid attraction to the tube wall to be sufficient for complete wetting of the inner tube surface. For this reason, we have added the criterion that when the wicking height of the liquid is equal to or greater than the diameter, stratified flow will not occur. The equation is:

$$R \leq \sqrt{\frac{2\sigma}{\rho_\ell g}} \tag{70}$$

Typical flow diagrams are shown in Figure 33. As can be seen, the boundaries between stratified and plug/slug flow, plug/slug and annular flow, stratified and annular flow, and annular and dispersed flow all move to lower mass velocities as the local acceleration is reduced. At very low gravitational accelerations, stratified flow will not appear. It should also be noted that at zero gravitational acceleration, the transition criteria do not work.

3. FUTURE AREAS OF INVESTIGATION

As shown in this section, the suggested transition criteria are not useful at "zero-g." Furthermore, their ability to predict flow regime shifts due to decreasing gravitational acceleration is questionable because of limited low gravity data. Therefore, this gap in the understanding of two-phase flow needs to be addressed. To do this, we would suggest looking at the relationships of the various forces and how lower acceleration levels would affect these relationships. This information could then be used to devise a method for modeling low gravity or zero gravity situations. At this point, actual "flight" data will be needed to compare the accuracy of the modeling method. Finally, all of this information can be combined so that ground testing of two-phase flows can be accurately extrapolated to low-g or zero-g conditions.

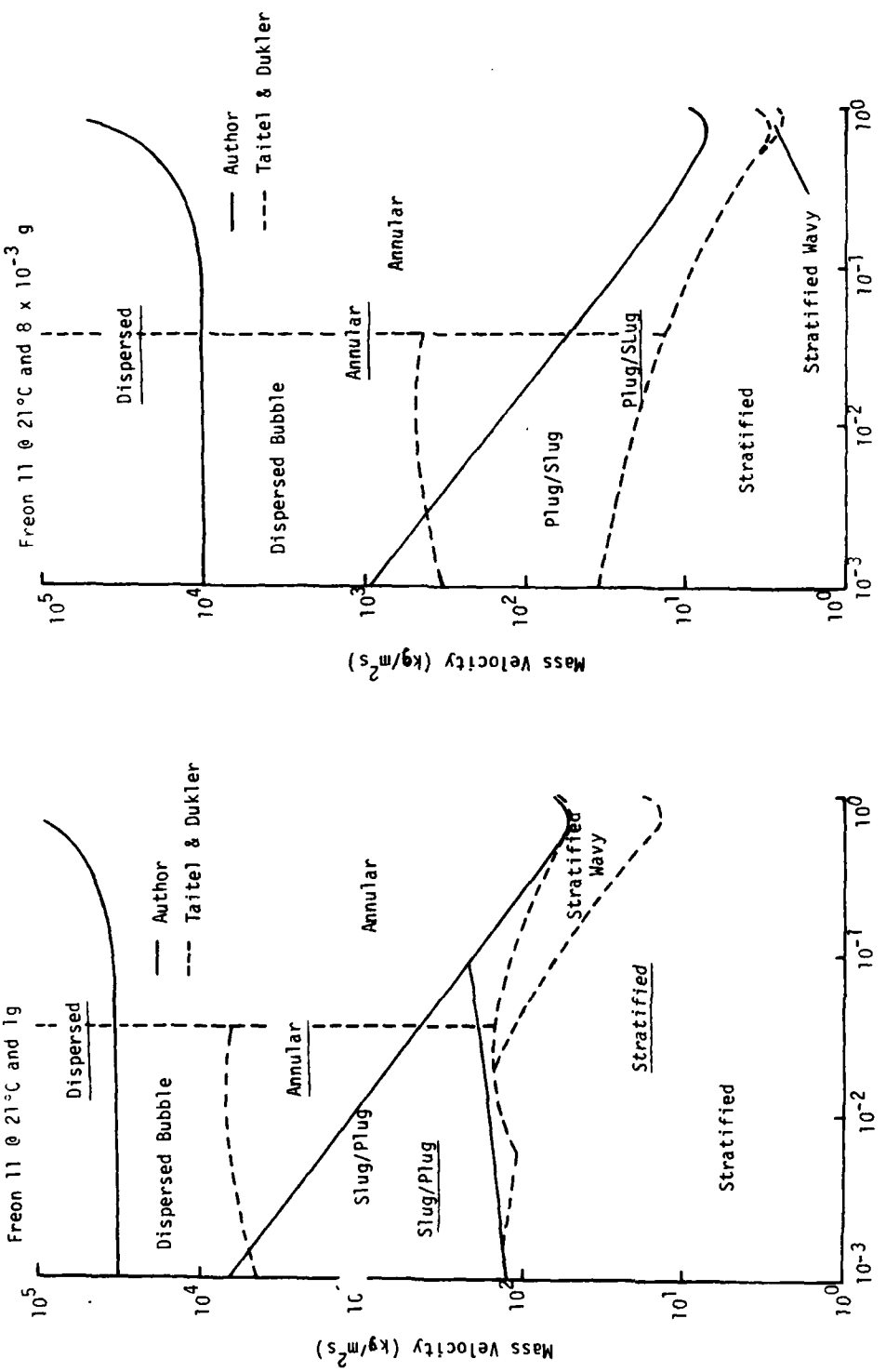

Figure 33. Typical Flow Regime Diagrams

SECTION V

THERMAL SYSTEM FACTORS

1. GENERAL CONSIDERATIONS

The preceding sections of this report were concerned with boiling, condensing, and two-phase flow processes. Using these processes in a closed loop thermal transport system will require an overall balance of fluid mass, energy, and momentum. Analytical tools for more accurate analysis of the system need to be developed as well as individual components such as evaporators and condensers. Initial concepts for these items will be discussed in later subsections.

Until additional data are generated, design of a two-phase fluid loop for operation in a weightless environment will be based on available theory and ground test correlations with very little data from actual zero-g flight tests. The probability of obtaining successful flight operation can be improved by testing prototype components and the assembled system in different orientations on the ground and/or designing the system to be relatively insensitive to gravitational effects. This insensitivity might be obtained by using high flow velocities resulting from either high mass flow rates or the use of swirl devices. Capillary or wick structures of various types can also be used to control the liquid location and obtain separation of liquid and vapor. However, one goal of continued development should be to establish a capability to design the simplest possible system so that weight, pump power, and fabrication costs are minimized.

2. LOOP CONCEPT EXAMPLES

Two examples are given below to illustrate possible concepts for implementation of two-phase fluid thermal transport loops. Brief consideration will be given to fluid selection and the type of components which might be used.

a. Space Station Thermal Loop

A tentative design approach has been selected for work under a NASA-sponsored contract (Reference 39) for initial development of thermal technology applicable to a future large space station. A basic schematic for this concept is shown in Figure 34 with values given for a 100 KW transport capability using refrigerant-11 (Freon-11) as the fluid. Flow modulation valves control the liquid flow to the evaporative heat exchangers so that load variations can be accomodated. Placing the loads in parallel allows independent temperature control so that variations of one load do not affect the other loads. In comparison to a single-phase liquid heat transfer loop for a 100 KW total load, calculations have shown that the two-phase R-11 loop would need only 1.5 percent of the input power for pumping and would have only 1.6 percent of the weight.

b. Satellite Thermal Loop Concept

The following concept is offered for a two-phase fluid thermal loop. This concept is suggested only as an aid in stimulating an exchange of information as it is nothing more than a pump-assisted heat pipe with separate vapor and liquid channels. The total system consists of pumps, evaporators, condensers, and an accumulator. The schematic of the system is shown in Figure 35.

The evaporators are based on a tunnel wick design patented by Thermacore, Inc. The wick consists of sintered, porous metal with tunnels running through it. This can be seen in Figure 36. The porous sintered wick offers high capillary pressure and excellent heat transfer characteristics while the tunnels create low flow-resistant paths for large flow rates. Use of a wicked evaporator provides increased parallel flow stability and passive heat load control. The increased stability results from the initial pressure drop in the evaporator. This pressure drop is recovered, however, through the wick because of the capillary pressure increase. The passive heat control occurs because the capillary pressure increase is related to the amount of liquid that is evaporated. With no heat load, the wick will saturate

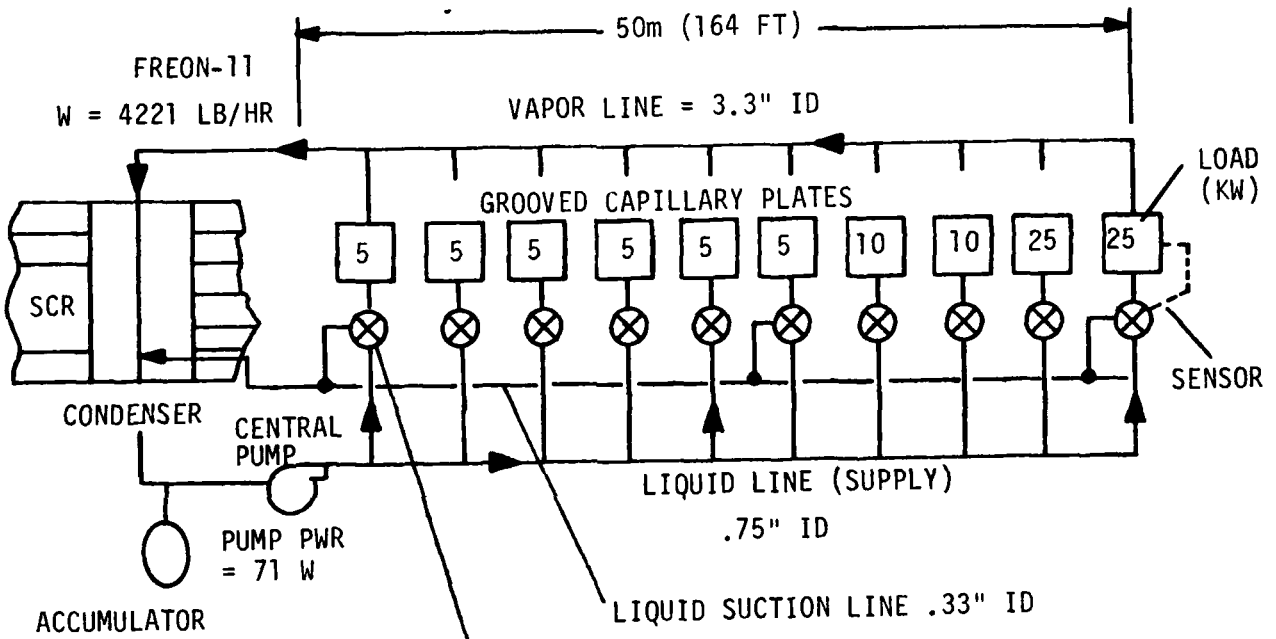

- TOTAL LOAD = 100 KW (t)
- WEIGHT (EXCLUSIVE OF SCR = 870 LB
- LOOP TEMP CONTROLLABLE: 4C to 40°C (39°F TO 104°F)
- LOOP TEMP BAND: 5°C (9°F)

Figure 34. Thermal Bus: Parallel Flow with Pump and Flow Modulation Valves

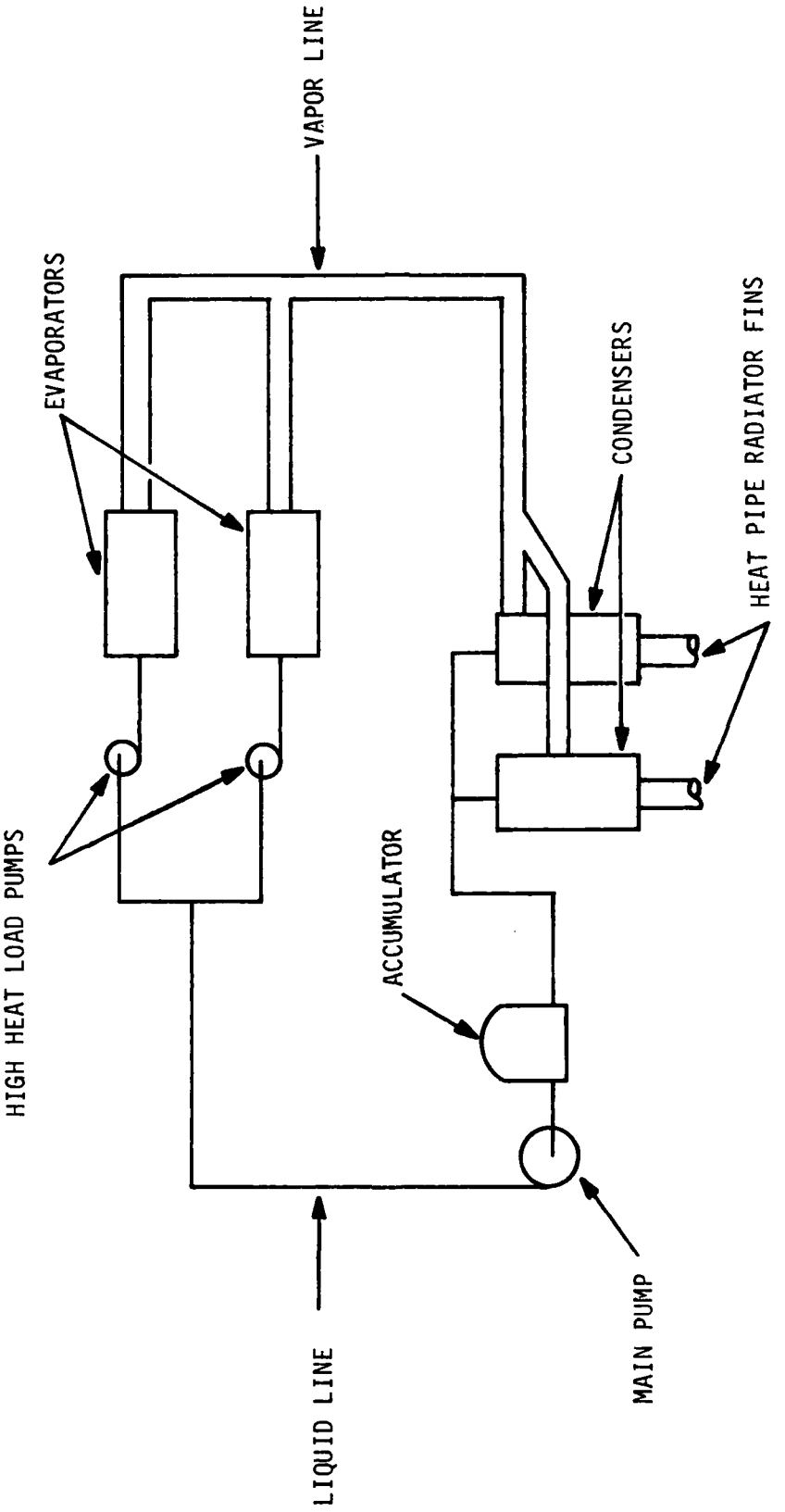

Figure 35. Two-Phase Thermal Transport Loop Concept

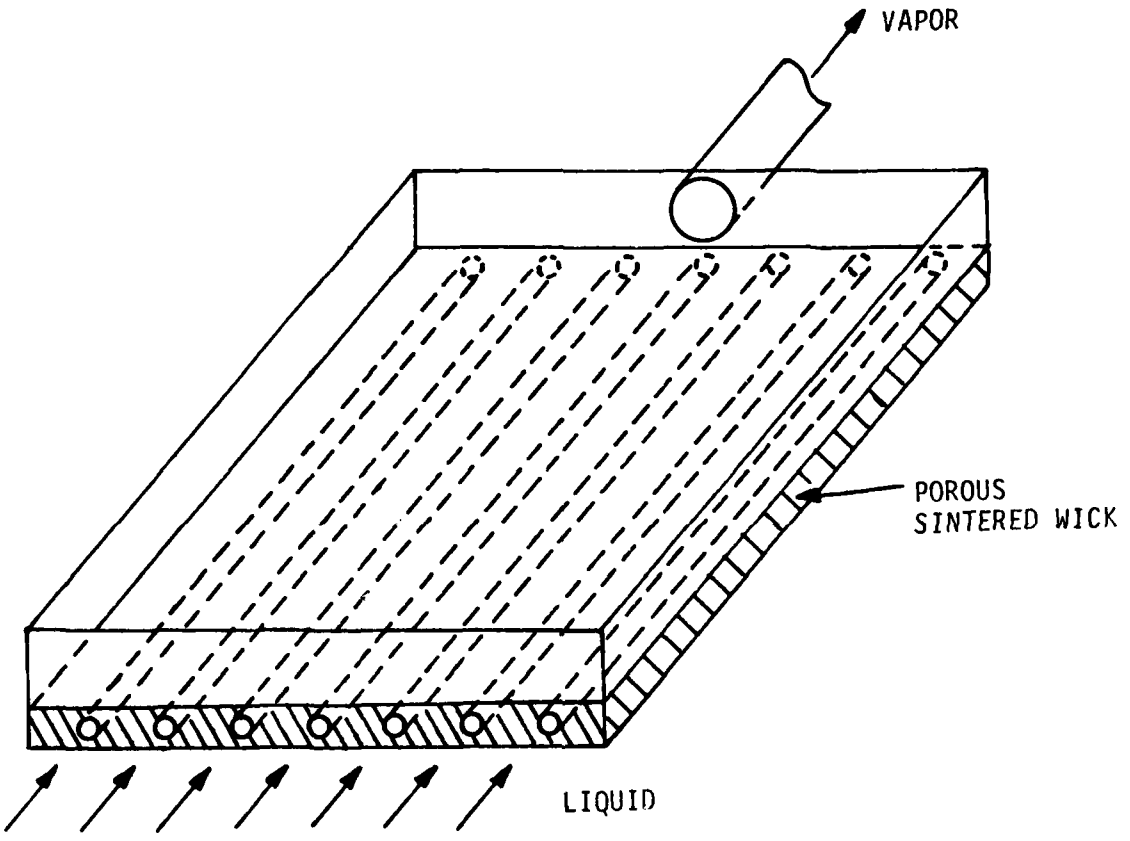

Figure 36. Evaporator Concept

and will not pump any fluid through it. As the heat load increases, the wick will pump more and more fluid. Eventually, with a high enough heat load, the capillary pumping action of the wick will be unable to supply enough liquid to the evaporator. Therefore, to increase the pulse heat load capability of the evaporator, high heat load pumps have been included so that additional liquid can be forced into the evaporators when needed.

The condenser shown in Figure 37 would be one of a set of condensers designed to mate with a heat pipe which is part of a radiator assembly. The condenser also employs the tunnel wick. Other wick designs are certainly possible for both the evaporator plates and the condenser.

The main pump would only have to make up for the pressure losses in the liquid portion of the loop. The vapor pressure drop should be taken care of by the capillary pressure increase.

The accumulator is necessary to insure that enough liquid is present for the system to operate for its entire life. It can also insure launch survivability by launching the loop dry and injecting the liquid from the accumulator into the main pump at start-up. This would ensure that problems would not develop because of liquid accumulation in the vapor lines during launch.

It can be seen from the above examples that components for the loops will need to be carefully developed. Several organizations are known to have concepts for evaporative heat exchangers, and a few designs have been tested in the laboratory. Much more work needs to be done to determine the type of condensers to be used in an eventual flight system. Design of these components would be substantially aided by a better understanding of two-phase fluid behavior in a weightless environment.

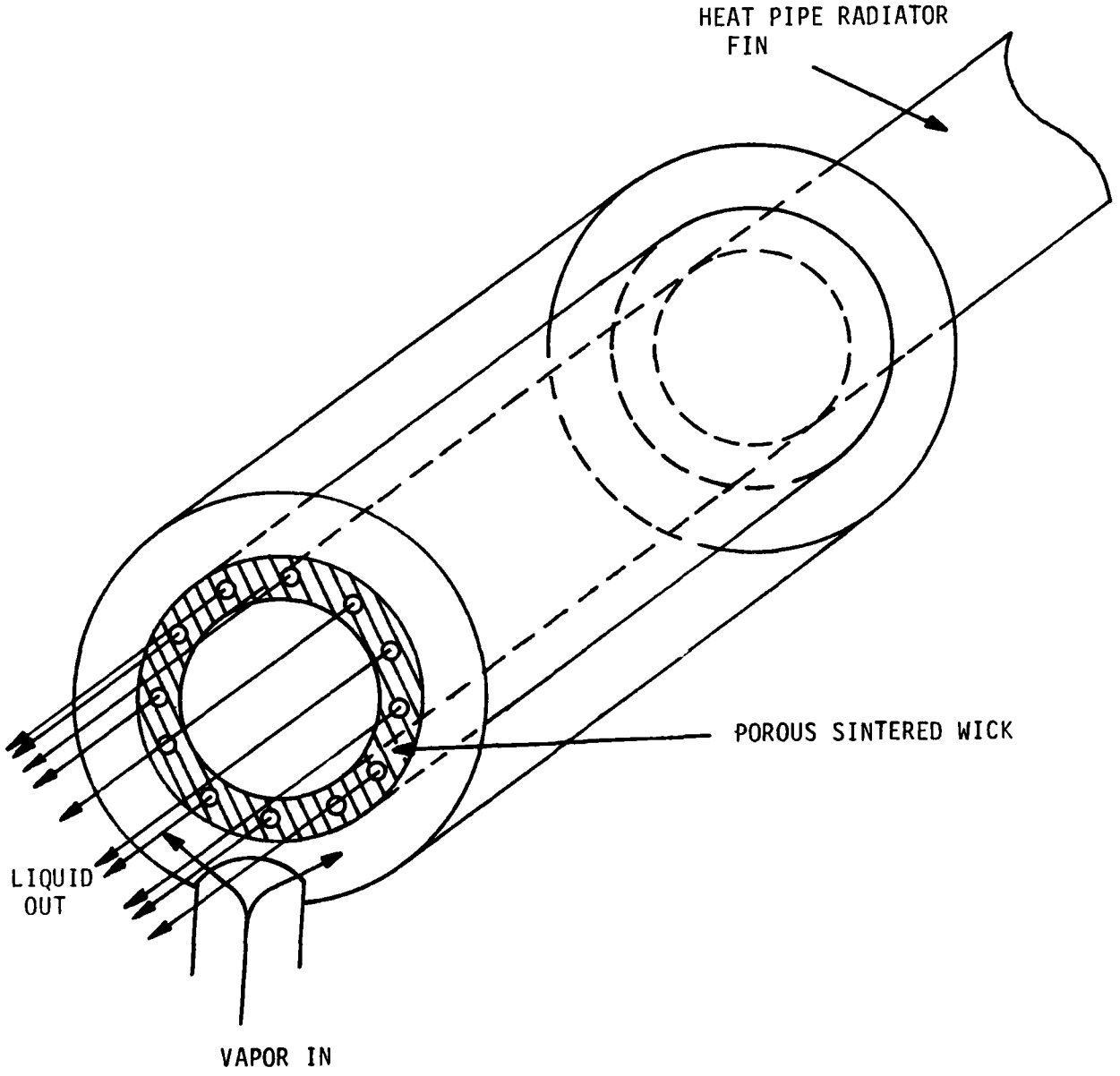

Figure 37. Condenser Concept

Earlier work (References 40 and 41) done by the Flight Dynamics Laboratory had shown that forced convection evaporators and condensers can be made to function in a weightless environment without the use of wicks. Straight-tube evaporators, tapered-tube condensers, vortex evaporator and a vortex condenser were all tested in zero-g aircraft flights. The main features of these experimental units are shown in Figures 38 and 39. Tests of the straight tube evaporator actually indicated a small increase in the boiling heat transfer coefficient during the zero-g part of the flight. This may have been caused by more effective wetting of the heated surface, but the precise reason should be investigated further. Performance of the vortex evaporators and condensers did not change significantly in going from one-g to zero-g. The tapered tube condenser also gave reliable performance. Preliminary tests with a straight tube condenser had indicated possible instabilities. However, later work (Reference 23) by NASA demonstrated zero-g condensation in small tubes.

One of the main goals of future work should be to establish the limits of zero-g phase change processes for simple geometries so that the use of complex devices for phase separation can be minimized in future spacecraft systems. This is desirable to reduce pumping power, lower costs, and improve reliability.

The particular fluid to be used in the heat transfer loop also needs to be determined. The three fluids of primary interest seem to be R-717 (ammonia), R-11, and R-114. Calculations done by several organizations indicate that use of ammonia would usually provide the lightest weight, lowest input power system. However, ammonia is somewhat difficult to use for laboratory experiments. Properties of the three fluids are listed in Table 2 for comparison at a temperature of 10°C (50°F). The table provides an indication of mass and volume flow rates to be expected for this type of system at three heat loads (5, 10, and 25 KW). Q_l is the liquid volume flow rate, and Q_v is the 100 percent quality volume flow rate.

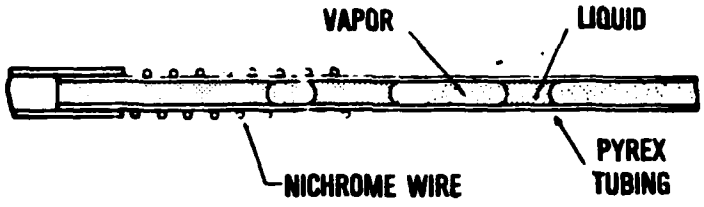

STRAIGHT TUBE EVAPORATOR

VORTEX EVAPORATOR

Figure 38. Non-Wicked Evaporators

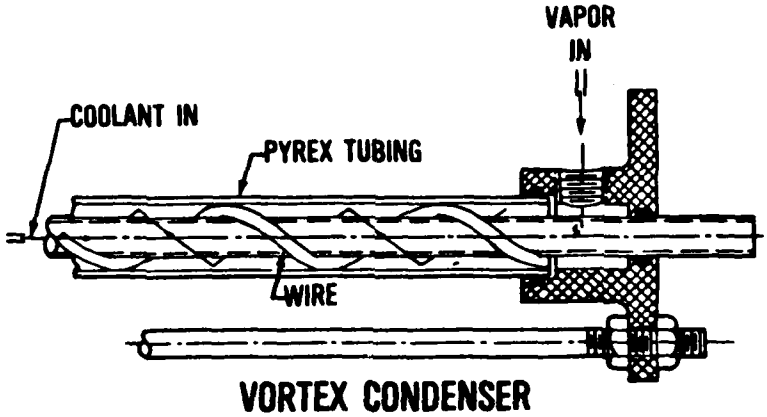

VORTEX CONDENSER

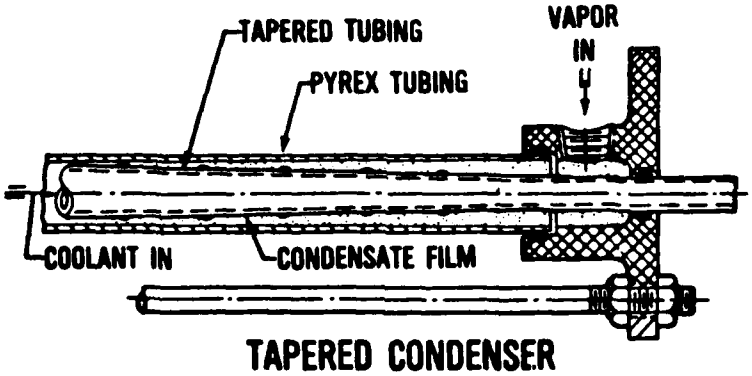

TAPERED CONDENSER

Figure 39. Non-Wicked Condensers

TABLE 2

SATURATED FLUID PROPERTIES AT 100 C (500F) (2830K)

Property	R-717 (Ammonia)	R-11	R-114
p - psia	89.19	8.783	18.53
- Nt/m^2	614,787	60,541	127,727
h_{lg} - j/g	1226.5	185.3	134.0
ρ_l - g/cm^3	.6248	1.511	1.501
ρ_v - g/cm^3	.004864	.003632	.009740
$\dot{m}$ - g/sec			
for 5 KW	4.077	26.98	37.31
for 10 KW	8.153	53.97	74.63
for 25 KW	20.38	134.9	186.6
$\dot{Q}_l$ - cm^3/sec			
for 5 KW	6.525	17.86	24.86
for 10 KW	13.05	35.72	49.71
for 25 KW	32.63	89.30	124.3
$\dot{Q}_v$ - cm3/sec			
for 5 KW	838.2	7428	3831
for 10 KW	1676	14,856	7662
for 25 KW	4190	37,140	19,155

As stated previously, a better understanding of two-phase fluid behavior is needed to furnish accurate design data. This improved data would then need to be incorporated into a computer program for analysis of the complete transport loop. Alternate loop arrangements could be compared, and optimum configurations derived. A tentative approach to eventually obtain better design data is outlined in the next subsection.

3. DESIGN DATA DEVELOPMENT APPROACH

One approach to developing more accurate methods for analysis of two-phase fluid systems is to determine the particular flow regimes which are expected to occur in each part of the system. Flow regime boundary prediction methods would be used to identify these flow patterns. The best available heat transfer, pressure drop, and stability equations could then be specified for each flow pattern. Careful use of these special equations could double the accuracy of analytical predictions compared to common practice using homogeneous models. The equations would be put into an appropriate form for computation and incorporated into computer program(s) to predict heat transfer rates and pressure gradients expected on a spacecraft compared to those observed in ground tests.

Based on expected conditions for a satellite heat transfer loop, and after detailed planning, experiments and tests need to be conducted to verify the analytical methods. A circulating loop with replaceable evaporators and condensers should be designed and assembled. The loop should be operable in both vertical and horizontal orientations. Experiments with transparent sections would verify expected flow regimes. Careful measurements of heat transfer rates and pressure drops would yield data for analytical correlation. Flow stability conditions could also be demonstrated. This is especially important when parallel evaporators or condensers are tested.

Special aspects of the advanced two-phase flow regime analysis will require extended periods of zero-g testing for final verification. This could possibly be done on space shuttle flights as a part of planned

NASA experiments. Details of these experiments will need to be derived as the analytical development proceeds.

The eventual goal is to be able to predict heat transfer coefficients and pressure gradients with an accuracy of about ten percent for both ground tests and space flight conditions. Values obtained with present analytical methods can be in error by 20 to 50 percent. This causes excess weight and power consumption to insure satisfactory operation with the uncertain performance characteristics. A significantly improved design approach will certainly be needed to obtain the potential benefits of using two-phase fluids for thermal transport on spacecraft.

Two-phase fluid work is, of course, only one aspect of the development of thermal management systems for future spacecraft. Other advanced components such as very lightweight radiators, thermal energy storage units, and automatic controls with microprocessors will also be needed.

SECTION VI

CONCLUSIONS

More effective and efficient thermal management methods will be needed on future military space satellites operating at higher energy levels for surveillance and defense missions. The use of two-phase fluid heat transfer loops can provide the needed transport capability with high efficiency and nearly uniform temperatures. Development of two-phase fluid systems for spacecraft has started, but a better understanding of the fluid behavior in a weightless environment (zero-g) is needed to ensure dependable performance.

Progress made at the Flight Dynamics Laboratory in beginning to expand the understanding of the phase change and flow processes is described in this report. Pool boiling may be possible at zero-g for fluids with a low surface tension in a sub-cooled liquid condition. Forced convection effects will aid the boiling process and reduce any difference between 1-g and zero-g performance. Condensation can also be made to occur with simple geometries in a weightless environment, but provision must be made to sweep the condensate film along the condensing surface. Flow patterns may be significantly different for zero-g operation, especially if small tubes are used. Effects on heat transfer coefficients and pressure gradients must be better understood to allow more accurate predictions for system design.

An approach to obtaining better analytical methods has been identified. This involves prediction of expected flow regimes so that heat transfer and pressure drop equations best suited for each particular flow regime can be used. These flow regime limits and corresponding equations would eventually be incorporated into computer programs for complete loop analysis. Considerable additional analytical and experimental work will be needed to formulate validated design methods.

This two-phase fluid work is only one aspect of thermal technology needed for future satellites. Lighter, more effective components will need to be developed and integrated into a complete energy management system.

REFERENCES

1. T. Mahefkey, "Military Spacecraft Thermal Management; The Evolving Requirements and Challenges," AIAA paper 82-0827, June 1982.

2. J. G. Rankin and P. F. Marshall, "Thermal Management System Technology Development for Space Station Applications," SAE Tech Paper 831097, presented at 13th ICES, July 1983.

3. S. Olendorf and F. A. Costello, "A Pumped Two-Phase Cooling System for Spacecraft," SAE Tech Paper 831099, presented at 13th ICES, July 1983.

4. D. C. Hustvedt and R. L. Oonk, Preliminary Design of Flight Hardware for Two-Phase Fluid Research, NASA CR-168072, February 1982.

5. Lord Rayleigh, Phil. Mag., Vol. 34, 94 (1917), (also see Reference 7).

6. Fritz, "Maximum Volume of Vapor Bubble," Physics Z, Vol. 36, 1935, pg. 379-384.

7. H. K. Forster and N. Zuber, "Growth of a Vapor Bubble in a Super-Heated Liquid," J. of Applied Physics, Vol. 25, No. 4, 1954, pg. 474-478.

8. H. K. Forster and N. Zuber, "Dynamics of Vapor Bubbles and Boiling Heat Transfer," A. I. Ch. E. J., Vol. 1, No. 4, 1955, pg. 531-535.

9. C. Han and P. Griffith, The Mechanism of Heat Transfer in Nucleate Pool Boiling, Report No. 7673-19, Massachusetts Institute of Technology, 30 March 1962.

10. E. G. Keshock and R. Siegel, Forces Acting on Bubbles in Nucleate Boiling Under Normal and Reduced Gravity Conditions, NASA TN D-2299, 1964.

11. R. Siegel and E. G. Keshock, "Effects of Reduced Gravity on Nucleate Boiling Bubble Dynamics in Saturated Water," A. I. Ch. E. J., Vol. 10, No. 4, 1964, pg. 509-517.

12. A. E. Bergles and W. M. Rohsenow, "The Determination of Forced Convection Surface Boiling Heat Transfer," J. of Heat Transfer, August 1964.

13. W. M. Rohsenow and J. P. Hartnett, Handbook of Heat Transfer, McGraw-Hill Book Co., New York, 1973.

14. W. R. Gambil, "Generalized Prediction of Burnout Heat Flux for Flowing Subcooled Wetting Liquids," Atch E, Preprint 17, 5th Nat. Heat Trans. Conf.

REFERENCES (Cont'd)

15. L. Bernath, "A Theory of Local-Boiling Burnout and Its Application to Existing Data," Chem. Engr. Prog. Symp. Ser., Vol 56, No. 30, pp 95-116, (1960)

16. J. G. Lavin and E. H. Young, Heat Transfer to Evaporating Refrigerants in Two-Phase Flow, A. I. Ch. E. J., November 1965.

17. M. Jacob, Heat Transfer, Vol. 1, John Wiley & Sons, Inc. New York, N.Y., 1956

18. J. C. Chen, "A Correlation for Boiling Heat Transfer to Saturated Fluids in Convective Flow," Ind. Engr. Chem. Process Des. Dev., Vol. 5, pp. 322-329, 1966.

19. C. E. Dengler and J. N. Addoms, "Heat Transfer Mechanism for Vaporization of Water in a Vertical Tube," Chem. Engr. Progress Symposium Series, Vol. 52(18), pp. 95-103, 1956.

20. See Reference 13.

21. W. H. Henstock and T. J. Hanratty, "The Interfacial Drag and the Height of the Wall Layer in Annular Flows," A. I. Ch. E. Journal, Vol. 22, November 1966.

22. John W. Miles, "The Hydrodynamic Stability of a Thin Film of Liquid in Uniform Shearing Motion," Journal of Fluid Mechanics, Vol. 8, August 1960.

23. J. L. Williams et al., "Development of a Direct Condensing Radiator for Use in a Spacecraft Vapor Compression Refrigeration System," Transactions of the ASME Paper No. 73-ENAS-5, 1973.

24. R. J. Deninton, Space Radiator Study, ASD-TR-61-697. (DDC No. AD-424-419), October 1963.

25. J. W. Palen, G. Breber, and J. Traborek, "Predition of Flow Regimes in Horizontal Tube-Side Condensation," Heat Transfer Engr., Vol. 1, No. 2, 1979, pp. 47-57.

26. T. N. Tandon, et al., "A New Flow Regimes Map for Condensation Inside Horizontal Tubes," Journal of Heat Transfer, Vol. 104, November 1982.

27. J. D. Keller, "Flow Distribution in Manifolds," Journal of Applied Mechanics, March 1949.

28. R. P. Krebs, H. C. Haller, and B. M. Auer, Analysis and Design Procedures for a Flat, Direct-Condensing, Central Finned-Tube Radiator, NASA TN D-2474, September 1964.

REFERENCES (Concluded)

29. D. B. Heppner, C. D. King, and J. W. Littles, "Zero-G Experiments in Two-Phase Fluid Flow Regimes," ASME Paper 75-ENAS-24.

30. L. S. Tong, Boiling Heat Transfer and Two-Phase Flow, John Wiley & Sons., Inc., 1965.

31. O. Baker, Simultaneous Flow of Oil and Gas," The Oil and Gas J., July 26, 1954, pp. 185-195.

32. M. Suo and P. Griffith, "Two-Phase Flow in Capillary Tubes," J. of Basic Engineering, September 1964, pp. 576-582.

33. E. Quandt, "Analysis of Gas-Liquid Flow Patterns," Chemical Engineering Progress Symposium Series, Vol. 65, No. 57, pp. 128-135.

34. See Reference 29.

35. Y. Taitel and A. E. Dukler, "A Model for Predicting Flow Regime Transitions in Horizontal and Near Horizontal Gas-Liquid Flow," A. I. Ch. E. Journal, Vol. 22, No. 1, pp. 47-55.

36. See Reference 4.

37. J. Weisman and S. Y. Kang, "Flow Pattern Transitions in Vertical and Upwardly Inclined Lines," International J. Of Multiphase Flow, Vol. 7, 1981, pp. 271-291.

38. J. Weisman, D. Duncan, J. Gibson and T. Crawford, "Effects of Fluid Properties and Pipe Diameter on Two-Phase Flow Patterns in Horizontal Lines," International J. of Multiphase Flow, Vol. 5, 1979, pp. 437-462.

39. Anan., Thermal Bus Subsystem for Large Space Platform, NASA-JSC Contract NAS9-16781 performed by Grumman Aerospace Co., 1983.

40. C. J. Feldmanis, Performance of Boiling and Condensing Equipment Under Simulated Outer Space Conditions, ASD-TDR-63-862, November 1963.

41. C. J. Feldmanis, "Pressure and Temperature Changes in Closed Loop Forced Convection Boiling and Condensing Processes Under Zero Gravity Conditions," Presented at the 1966 Annual Technical Meeting of the Institute of Environmental Sciences.

U.S.Government Printing Office: 1984 -- 559-065/50529